Thermal fluctuations independently modulate physiological plasticity and the dynamics of the gut microbiome in a tropical rocky shore oyster

Bovern Suchart Arromrak[1]; Adrian Tsz Chun Wong[1]; Tin Yan Hui[1]; Kin Sum Leung[1]; Gray A. Williams[1]; Monthon Ganmanee[2]; Thierry Durand[3]; Jetty Chung Yung Lee[4]; & Juan D. Gaitan-Espitia[1*]

[1] The Swire Institute of Marine Science and School of Biological Sciences, The University of Hong Kong, Hong Kong, SAR, China.

[2] Department of Animal Production Technology and Fisheries, Faculty of Agricultural Technology, King Mongkut's Institute of Technology Ladkrabang, Bangkok 10520, Thailand

[3] Institut des Biomolécules Max Mousseron (IBMM), Pôle Chimie Balard Recherche, UMR 5247, Université de Montpellier, CNRS, ENSCM, F-34293 Montpellier Cedex 05, France

[4] School of Biological Sciences, The University of Hong Kong, Hong Kong, SAR, China

*** Correspondence**: juadiegaitan@gmail.com

Abstract

Extreme high thermal conditions on tropical rocky shores are challenging to the survival of intertidal ectotherms. Yet, many species are highly successful in these environments in part due to their ability to regulate intrinsic mechanisms associated with physiological stress and their metabolic demand. More recently, there has been a growing awareness that other extrinsic mechanisms, such as animal-associated microbial communities, can also influence the tolerance and survival of ectotherms under stressful conditions. However, the extent to which the intrinsic and extrinsic mechanisms are functionally linked as part of the overall adaptive response of intertidal animals to temperature change and stress is poorly understood. Here, we examined the dynamics and potential interactions of intrinsic and extrinsic mechanisms in the tropical high-supratidal oyster, *Isognomon nucleus*. We found that oysters modulate their internal biochemistry (oxidized PUFA products, including 5-F_{2t}-IsoP, 10-F_{4t}-NeuroP, 13-F_{4t}-NeuroP, and 16-F_{1t}-PhytoP) as part of their adaptive regulation to cope with physiological stress during periods of extreme high temperatures when emersed. However, while we detected variation in alpha diversity (ASV richness and Shannon diversity index), dominant microbial taxa and microbial functions across time, no association was found with the host biochemical profiles. The findings here suggest that the thermal condition within oysters can independently influence their intrinsic biochemical responses and extrinsic microbiome profiles. Together, these mechanisms may contribute to the thermal tolerance and survival of the oysters in the challenging conditions of the tropical high-supratidal zone.

Keywords: Phenotypic plasticity, ectotherms, microbiome, thermal stress

Introduction

The tropical rocky shore is one of the most extreme environments on Earth. This system is characterized by a marked heterogeneous thermal landscape influenced by tidal dynamics (Raffaelli and Hawkins, 1999; Helmuth and Hofmann, 2001). Across this vertical gradient

44 defined by the tides, environmental temperatures shape the physiology, behaviour, and spatial
45 distribution of tropical intertidal ectotherms (Garrity, 1984; Williams and Morritt, 1995; Chow,
46 2004; Samakraman *et al.*, 2010; Giomi *et al.*, 2016; Ng *et al.*, 2017). For ectotherms occupying
47 the high intertidal zone (hereafter, high-supratidal zone), thermal and oxidative stress (i.e.,
48 excessive production of reactive oxygen species - ROS) during desiccation periods of extended
49 emersion, are the two of the major physiological challenges faced (Sokolova and Pörtner, 2001;
50 Freire *et al.*, 2011; Birben *et al.*, 2012).

51 To survive under these challenging conditions, high-supratidal ectotherms modulate
52 intrinsic/innate mechanisms associated with their internal physiology (e.g., metabolic rate) and
53 biochemical activities. This modulation can be observed through, for instance, the removal of
54 ROS via polyunsaturated fatty acids (PUFA; Sokolova and Pörtner, 2001; Yin *et al.*, 2017;
55 Monroig *et al.*, 2022), and/or the control of the gene expression associated with heat shock
56 response (HSR) and oxidative stress response (OSR; Wang *et al.*, 2022). PUFAs such as
57 Arachidonic acid (ARA) and Docosahexaenoic acid (DHA) are known to be effective
58 molecules and agent for ROS removal, because they contain unsaturated double bonds making
59 them susceptible to ROS reaction (particularly to peroxide, HO•) (Sargent, 1976; Leung *et al.*,
60 2015; Yin *et al.*, 2017; Fadhlaoui and Lavoie, 2021). The non-enzymatic peroxidation of these
61 PUFAs, generates by-products that can be used as biomarkers of the ROS level (Miller *et al.*,
62 2014; Yonny *et al.*, 2016; Galano *et al.*, 2017). In addition to the biochemical modulation
63 mechanism, some intertidal organisms (e.g., the oysters, *Isognomon nucleus*) are able to enter
64 into a hypometabolic state (i.e., metabolic depression, for instance, marked by a drop in heart
65 rate; Marshall and McQuaid, 2011; Hui *et al.*, 2020) to avoid excessive energy consumption
66 when exposed to high temperatures during low tides. Together, these functional characteristics
67 are regarded as important adaptive traits for intertidal ectotherms to cope and ameliorate the
68 extreme stress experienced on tropical rocky shores.

69 Survival under stressful environmental conditions is also hypothesized to be influenced
70 by extrinsic/acquired mechanisms such as host-associated microbial communities (i.e.,
71 microbiome; Bang *et al.*, 2018; Ahmed *et al.*, 2019). The structure and functions of these
72 microbiomes have been suggested to play important roles in shaping tolerances and
73 biochemical regulation of animals to elevated temperatures (Herrera *et al.*, 2020; Sepulveda
74 and Moeller, 2020; Jaramillo and Castañeda, 2021). Under such conditions, functional
75 microbiomes that are resilient/responsive to environmental changes are fundamental to the
76 host's health and survival (Soen, 2014; Kremer *et al.*, 2018). For instance, Epstein et al. (2019)
77 demonstrated that the resilience of the coral, *Pocillopora acuta,* to a stressful thermal event
78 may be attributed to the stability of the microbiome composition and structure. In contrast, a
79 dysbiotic host state is commonly associated with a destabilized microbiome (Fan *et al.*, 2013;
80 McDevitt-Irwin *et al.*, 2019). This is typically reflected by a marked variation among host-
81 associated microbiomes, a signal indicating the host losing control of the microbial community
82 (e.g., increase in opportunistic pathogens) and/or differential sensitivities of microbiomes to
83 extreme disturbances (e.g., elevated temperature; Carey and Duddleston, 2014; Petersen and
84 Round, 2014; Lokmer and Wegner, 2015). This pattern is in-line with the "Anna Karenina
85 Principle", which states, "all happy families are all alike; each unhappy family is unhappy in
86 its own way" (Zaneveld *et al.*, 2017; Díaz-Almeyda *et al.*, 2022). In other words, stressed
87 organisms may host more stochastic microbiomes than healthy organisms. Although
88 microbiome stability seems important for host homeostasis, some studies have suggested that
89 flexibility in the microbiome can also provide adaptive capacities to the host, allowing it to
90 cope with rapidly changing environments (Maher *et al.*, 2020; Voolstra and Ziegler, 2020).
91 Ziegler et al. (2017), for example, showed that the coral *Acropora hyacinthus* exhibits changes
92 in its microbiome composition and structure that are aligned with the local thermal
93 environmental conditions. Similarly, several studies have also shown seasonal variation in the

94 host-associated microbiome of many marine organisms such as bivalves and echinoderms, as a
95 potential plastic/flexible response to environmental change (Pierce and Evan, 2019; Feng *et al.*,
96 2021). Microbiome stability or flexibility may, therefore, be a sign of host adaptive responses
97 to environmental changes. However, the influence of these contrasting patterns is context-
98 dependent and thus, their contribution to the tolerances and survival of animal hosts may differ
99 in thermally challenging environments such as tropical rocky shores.

100 Previous studies have shown that the capacity for plastic adaptive responses of animal
101 hosts to environmental stress may be modulated by the interactions between intrinsic
102 (physiology and biochemical changes of the host) and extrinsic (host's microbiome structure
103 and function) mechanisms (Muñoz *et al.*, 2019; Marangon *et al.*, 2021; Fontaine and Kohl,
104 2023). It is unclear, however, to what extent these mechanisms are functionally linked as part
105 of the whole organism's adaptive response (i.e., holobiont: host and microbiome) to survive in
106 an extreme environment such as the tropical intertidal rocky shore. In this study, we
107 investigated the intrinsic and extrinsic mechanisms underpinning the tolerances and survival of
108 a tropical intertidal ectotherm (oyster, *Isognomon nucleus*) by assessing the influence of natural
109 variation in environmental temperature on i) host physiology (i.e., biochemical dynamics) ii)
110 the diversity, structure, and function of the host gut-associated microbiome and iii) the interplay
111 between these mechanisms. The integration of intrinsic and extrinsic mechanisms offers a
112 holobiont perspective for understanding the stress tolerance regulation of ectotherms in extreme
113 high temperature and fluctuating environments (Alberdi *et al.*, 2016; Apprill, 2017; Bang *et al.*,
114 2018).

115 Materials and methods

116 *Site and species descriptions*

117 Host-microbiome interactions were investigated in the oyster, *Isognomon nucleus*
118 (Bivalvia: Isognomonidae), a dominant ectotherm of the high-supratidal zone in Southeast Asia.

119 Animals were collected from Ko Sichang, Thailand (latitude: 13°08'52''N; longitude:
120 100°48'11''E). In this area, *I. nucleus* is abundant and forms a distinctive band at the high-
121 supratidal zone (~2.5 - 3 m above the mean sea level; Samakraman *et al.*, 2010), where rock
122 temperatures vary daily (emersion period) from ~30°C at dawn to ~50°C at noon (hot season:
123 March to June; Hui *et al.*, 2020). The oyster exhibits strong variations in physiological and
124 metabolic adjustments with elevated body temperatures, providing an ideal system to
125 investigate the functional role of the microbiome to facilitate the host's survival in this
126 thermally extreme and variable environment (Giomi *et al.*, 2016; Hui *et al.*, 2020).
127

128 *Sample collection and processing*

129 A total of 80 individuals of *I. nucleus* were randomly selected at four different
130 timepoints within an emersion period (Fig. 1A; 20 animals at each time). These timepoints
131 (09:15 hr, 12:30 hr, 16:12 hr, and 17:40 hr; hereafter, morning, noon, early-afternoon, and late-
132 afternoon, respectively), encompass a temporal cycle characterized by major changes in the
133 environmental temperature (Table S1) as a result of the tidal dynamics and air/sun exposure
134 (Hui *et al.*, 2020). Body temperatures were measured from 10 randomly selected individuals at
135 each timepoint using a digital thermometer (± 0.1 °C, TM-947SD, Lutron, Taiwan) where a
136 fine-tipped type-K thermocouple was inserted into the bodies through the valve opening. At
137 each time point, the whole tissue of five collected oysters was quickly removed at the site with
138 a sterile dissecting kit and snap-frozen in liquid nitrogen on shore for oxidative stress
139 quantification (as a proxy for host physiological and biochemical dynamics). The guts of
140 another five individuals were also dissected at each timepoint on-site, snap frozen in liquid
141 nitrogen for gut microbiome assessment. All collected samples (20 for oxidative stress and 20
142 for microbiome analysis across four time points) were stored in a portable liquid nitrogen tank
143 and transported to The University of Hong Kong within three days, where they were held in a
144 -80°C freezer until processing and analyses. Because of the weather instability and strong waves

during the fieldwork, temporal sampling was limited to one day to comply with logistic and safety regulations.

Rock surface temperature and tidal dynamics

To quantify environmental conditions experienced by *Isognomon nucleus* throughout the tidal cycle, rock surface temperatures and tidal levels were recorded. To measure and track surface rock temperature, i-Button loggers (DS1922L, Maxim, US) were firstly embedded in waterproofing resin (Scotchcast, 3M, US), placed in plastic Falcon tube caps and affixed, using marine epoxy (A-788, Z-Spar, US; Ng *et al.*, 2021), onto the shore at the height where *I. nucleus* were collected. Rock surface temperatures were logged by these i-Buttons every 5 minutes at a resolution of 0.5 °C (n = 5). Additionally, a time-lapse camera (TLC200Pro, Brinno, Taiwan) was set adjacent to the study site to monitor the immersion state of the *I. nucleus* band during the day (~ 05:00 hr to 18:00 hr) to assess the tidal states. Images were captured every 10 minutes and the tidal level was scored according to whether the band was underwater (immersed), exposed to air (emersed), or being splashed by waves during transitions from immersion/emersion (awash). During the emersion period, animals showed no intermittent gaping (Hui, T.Y., unpublished data). Predicted tide height from the lowest low water height on the sampling date was also obtained from the Hydrographic Department, Royal Thai Navy Website (https://www.hydro.navy.mi.th/index1.php#nogo2): Lowest tidal height – 0.55m (12:56 hr) and highest tidal height - 3.36m (20:53hr).

Determination of oxidized polyunsaturated fatty acids products

The levels of oxidative stress (i.e., associated with ROS production) of the oysters were determined based on the concentration of non-enzymatic oxidized polyunsaturated fatty acids (PUFA) products (hereafter, oxidized PUFA products; Durand *et al.*, 2009; Basu, 2010; Leung *et al.*, 2015). These oxidized products are derived from phospholipids in the membranes, hence

172 require hydrolysis for measurement. A modified Folch extraction method was used to extract
173 the oxidized PUFA products from the oysters sampled (n=5) at each timepoint (t=4) (Folch *et*
174 *al.*, 1957; Dupuy *et al.*, 2016). In brief, 0.05g of oyster flesh was suspended in a 5 ml ice-cold
175 Folch solution (chloroform: methanol, 2:1, v/v) with 0.01% Butylated HydroxyToluene (BHT;
176 used as anti-oxidant to prevent lipid peroxidation during sample processing) (w/v) and
177 homogenized at 24,000 rpm in 20 secs bursts on ice using a polytron benchtop homogenizer
178 (T25, Ultra-Turrax, IKA, Germany). Homogenization was performed twice, and the two parts
179 of the Folch solution extracts were pooled. The pooled solutions were added with 2 ml of 0.9%
180 NaCl to introduce phase separation. The mixture was then shaken on ice for 30 min and
181 centrifuged at 2000 × g for 10 min at room temperature. The lower chloroform phase was
182 transferred into a 30 ml glass vial. The extracted samples were then added with potassium
183 hydroxide (1M in methanol) and 1X PBS (pH7.4). Samples were then shaken overnight in the
184 dark at room temperature for alkaline hydrolysis of the extracted samples. The reaction was
185 terminated by adding 1M of hydrochloric acid, methanol, 20 mM of formic acid, and 40 mM
186 of formic acid. Deuterated internal standards (5ng prepared in methanol) were also added after
187 the hydrolysis. Purification of the oxidized PUFA metabolites was performed with the mixed
188 anion solid phase extraction (MAX SPE, Waters, Milford, MA USA). Before the start of the
189 solid phase extraction, the SPE column was preconditioned with methanol and 20 mM formic
190 acid. One sample was then loaded into a column and cleaned with 2% ammonium hydroxide
191 and 20 mM formic acid. The final eluent was collected with hexane/ethanol/acetic acid
192 (70/29.4/0.6, v/v/v). All the samples were then placed on a heating block and heated at 37°C
193 under a stream of nitrogen gas until they were completely dried. The dried samples were then
194 re-suspended in 100 µL methanol and cleaned through a 0.45 µm PTFE filter to remove
195 insoluble impurities, and then immediately analysed by liquid chromatography-tandem mass
196 spectrometry (LC-MS/MS).

197 In our study, we used the Sciex X500R QTOF LC-MS/MS system (Sciex Applied
198 Biosystems, MA, USA) which consisted of an Exion LC liquid chromatography with a C18
199 column (150×2.1 mm, 2.6 µm particle size, Phenomenex, Torrance, CA, USA) which was
200 maintained at 40°C for LC-MS/MS analysis. A mobile phase consisting of 0.1% aqueous acetic
201 acid (solvent A) and 0.1% acetic acid/methanol (solvent B) was used. The flow rate was set to
202 300 µl/min and the injection volume to 10 µl. For each sample analysis, the gradient condition
203 was maintained at 20% of solvent B for 2 min and between 20% and 98% for 8 min and then
204 held for 5 min. Then, the percentage of solvent B was reduced to 20% in 1 min and held for an
205 additional 5 min to equilibrate to the initial conditions. The X500R QTOF system was operated
206 in negative electrospray ionization (ESI) mode. The spray voltage was set to -4500V and
207 nitrogen was used as the curtain gas. The ionization chamber temperature was set at 350°C, and
208 the pressure of the ion source gases 1 and 2 were 35 and 45 psi, respectively. The declustering
209 potential (DP) was set to -80V and the collision energy (CE) was -10V for the QTOF MS. The
210 scan mode was set to multiple reaction monitoring (MRM). All data collected by the X500R
211 QTOF system was analyzed by the Sciex operating system (version 1.2.0.4122). The
212 quantification of each analyte was determined by correlating the peak area to its corresponding
213 deuterated internal standard peak. For analytes without corresponding deuterated internal
214 standards, the following deuterated internal standards, 5(*S*)-HETE-d_8, 15-F_{2t}-IsoP-d_4, and 4-F_{4t}-
215 NeuroP-d_4 were used for quantification. We identified fifteen oxidized PUFA products that are
216 known to be the products of non-enzymatic lipid peroxidation (Table S2), based on previous
217 work by Dupuy et al.(2016), Galano et al.(2017) and Lee et al.(2018).
218
219 *DNA extraction and 16S rRNA gene sequencing*
220 Total genomic DNA was extracted from the oysters' guts (~0.03g) using the commercial
221 DNA extraction kit, Dneasy Power Soil Kit (Qiagen GmbH, Hilden, Germany), following the
222 manufacturers protocol with some modifications (i.e., the solution mixture was incubated at 55°C

223 in a water bath for 30 minutes after the bead-beating step). The extracted DNA (100µl) was
224 then collected in a microcentrifuge tube and preserved in a -80°C freezer. All the DNA samples
225 were then sent to Ramaciotti Centre for Genomics at the University of New South Wales,
226 Sydney Australia for 16S rRNA amplicon paired-end sequencing (2X 300bp) on an Illumina
227 Miseq Platform. Before the amplicon sequencing, the V3-V4 variable region of the 16S rRNA
228 gene from each DNA sample was amplified using the following primers: (1) 341F (Forward
229 Primer);5'- CCTACGGGNGGCWGCAG-3' (2) 805R (Reverse Primer); 5'-
230 GACTACHVGGGTATCTAATCC-3'(Herlemann *et al.*, 2011; Klindworth *et al.*, 2013). Raw
231 reads received were the demultiplexed paired-end sequences in a FASTQ format and they were
232 deposited in NCBI Sequence Read Archive (SRA) under Bioproject number PRJNA931123.
233 The data will be made available once published.
234

235 *16S rRNA gene sequence processing*

236 Raw demultiplexed paired-end sequences were processed following the Quantitative
237 Insights into Microbial Ecology (QIIME2 ver. 2021.4) pipeline (Bolyen *et al.*, 2019). Briefly,
238 the raw data was first visualized with the demux plug-in function for quality-checking and
239 identifying poor-quality base regions to filter. The sequences were then trimmed, filtered,
240 denoised, chimeras-removed, and merged using the DADA2 plug-in function in QIIME2
241 (Callahan *et al.*, 2016). The sequences were identified at a single nucleotide threshold
242 (Amplicon Sequence Variants; ASV; Callahan *et al.*, 2017). Additional steps of quality control
243 were performed to reduce non-target sequences by aligning (vsearch alignment method) the
244 ASV sequences to the 99% representative sequences from the greengenes database and only
245 ASV with a similarity threshold of 0.65% and coverage threshold of 0.5% were retained
246 following https://github.com/biocore/deblur/issues/139#issuecomment-282143373. Singletons
247 and sequences with less than 349bp were also removed with filter-features and filter-sets

248 function in QIIME2, respectively. The quality-filtered sequences were then taxonomically
249 assigned with a naïve-Bayes classifier trained on the V3-V4 region of the 16S gene in the Silva
250 v138 database (Quast *et al.*, 2013), using the classify-sklearn function in the feature-classifier
251 plugin (Bolyen *et al.*, 2019). The output from this generated a taxonomy table with taxonomic
252 naming for each ASV found within our samples. ASV sequences that were identified as
253 mitochondria, chloroplast, archaea, and eukaryotes were filtered out. The quality-filtered ASV
254 sequences were then ready to be used for downstream analysis.
255

256 *Profiling microbiome functions*

257 The functional microbiome was predicted using the software Phylogenetic Investigation
258 Communities by Reconstruction of Unobserved States version 2 (PICRUSt2; Douglas *et al.*,
259 2020). The predicted functions associated with the microbiome (using the quality-filtered
260 sequences) were inferred based on the MetaCyc pathway abundance, using the PICRUSt plug-
261 in within QIIME2.
262

263 *Data analysis*

264 Unless otherwise specified, the R statistical programming language (ver. 4.2.0, R Core
265 Team) and R Studio was used to generate graphics and statistical analyses. The oysters' body
266 temperature data violated the statistical assumption of homogeneity of variances (Levene's test,
267 p-value < 0.05). Hence, the statistical analysis for this trait across different timepoints was
268 assessed using a generalized linear model (GLM) with a gamma distribution. The likelihood-
269 ratio chi-square test was used to determine the statistical significance and is indicated if the p-
270 value was < 0.05 (R package "Car"; Fox and Weisberg, 2019). Post-hoc testing for pairwise
271 comparison was made using the estimated marginal means with Tukey's tests from the R
272 package emmeans (Lenth, 2023)

273 Individual oxidized PUFA products were first evaluated for normality (Shapiro-Wilk's
274 Test) and homogeneity of variance (Levene's test) assumptions. Metabolites that fulfilled both
275 assumptions were tested with one way Analysis of variance (ANOVA) to investigate the
276 variation in metabolites' concentrations across timepoints, followed by *post-hoc* Tukey's
277 Honest significant difference (Tukey's HSD). For metabolites that violated either one of the
278 assumptions, they were evaluated with GLM (gamma distribution) following a similar
279 procedure as with the body temperature datasets.

280 Assessment of oxidized PUFA products' beta diversity (with all the 15 metabolites or
281 only the 4 significant metabolites) was performed by first generating a Euclidean distance
282 matrix between samples, using normalized metabolites datasets (i.e., autoscaling; van den Berg
283 *et al.*, 2006). Euclidean distance metric was selected as it allows for accurate and reliable
284 analysis for continuous datasets and testing the differences between groups of samples based
285 on the metabolite data (Qi and Voit, 2017; Mallick *et al.*, 2019; Nguyen *et al.*, 2021). A
286 principle Coordinate Analysis (PCoA) plot was then created to visualize the oxidized PUFA
287 products clustering across different timepoints, using the ggplot2 R package (Wickham, 2008).
288 Permutational multivariate analysis of variance (PERMANOVA) was performed with 999
289 permutations to test for the differences in oxidized PUFA products profile across timepoints
290 (Oksanen *et al.*, 2022). We also performed a permutational multivariate dispersion test
291 (PERMDISP) to assess differences in the dispersion of metabolite profiles between timepoints
292 with 999 permutations followed by pairwise comparisons. All multivariate metabolites analyses
293 were performed using the package vegan in R (Oksanen *et al.*, 2022).

294 Oysters' gut microbiome analysis was conducted by first combining the ASV count data,
295 taxonomy table, and metadata into a simplified data matrix for ease of downstream processing,
296 using the phyloseq() function from the phyloseq R package (McMurdie and Holmes, 2013).
297 Rarefaction curves (total ASVs captured against sampling depth) were generated for each

298 sample with the ggrare() function from the ranacapa R package (Kandlikar *et al.*, 2018). All
299 samples approached the asymptote level, indicating that the total ASV richness for each sample
300 has been captured (Fig. S1). Each of the samples was then rarefied to a sampling depth of
301 21,282 reads (a cut-off that balances the maximum number of sequences retained per sample
302 and minimizing the number of samples removed) for downstream analysis (Weiss *et al.*, 2017;
303 i.e., alpha and beta diversity; McKnight *et al.*, 2019). Using the rarefied data, the microbiome
304 alpha diversity (i.e., the structure of a microbial community with respect to its richness and
305 evenness; Willis, 2019) was determined based on two indices – ASV richness (based on the
306 number of ASV present within a group) and Shannon-Wiener (H') diversity (based on both, the
307 number of ASV and their abundances within a group). ASV richness was calculated with the
308 Base-R function, while Shannon-Wiener (H') diversity index was generated using the diversity()
309 function from the Vegan package (Oksanen *et al.*, 2022). Differences in the microbiome alpha
310 diversity across the timepoints were assessed with ANOVA and followed by a *post-hoc* Tukey
311 HSD test. The ANOVA statistical assumptions of normality (Shapiro-Wilk test) and
312 homogeneity of variance (Levene's test) for all datasets were tested and fulfilled (p-value >
313 0.05). Linear regression analysis was also conducted to determine the relationship between the
314 oysters' microbiome alpha diversity (i.e., ASV richness and Shannon-Wiener (H') index) and
315 body temperature (i.e., average of the 10 random independent body temperature replicates
316 collected at each timepoint). The statistical assumptions for the linear regression model were
317 fulfilled based on the normality test (Shapiro-Wilk test) and residuals plot (variance
318 homogeneity).

319 While alpha diversity focuses on community variation within a community (sample),
320 beta diversity quantifies (dis-)similarities between communities/samples in terms of species
321 presence/absence and abundance (Kers and Saccenti, 2022). Metrics of beta diversity are
322 typically used to measure species turnover or replacement across different locations,

323 environmental conditions or timepoints (Kers and Saccenti, 2022). Here, we assessed beta
324 diversity of the oysters' gut microbiome to evaluate temporal differences in taxonomic and
325 functional structure across all samples simultaneously. Bray-Curtis dissimilarity distance
326 matrix was first generated between all samples. Then, a PCoA plot was created to visualize
327 microbiome taxonomic and functional clusters across different timepoints, using the ggplot2 R
328 package (Wickham, 2008). The chosen dissimilarity distance metric (Bray-Curtis) followed
329 findings by Mcknight et al. (2019) and Weiss et al. (2017), in which authors showed optimal
330 and high confidence for community level comparison with rarefied microbiome datasets.
331 PERMANOVA was performed with 999 permutations to test for the differences in the
332 microbiome composition and structure between timepoints (Oksanen *et al.*, 2022). PERMDISP
333 with 999 permutations was performed to test for differences in the taxonomic and functional
334 microbiome profile dispersion followed by pairwise comparison. All multivariate analyses
335 were conducted using the package vegan in R.

336 Differential abundance analysis of each microbial taxa was performed with family
337 taxonomic level data (using unrarefied quality-filtered ASV sequences) and analysed with
338 Analysis of Composition Microbiome with Bias Correction (ANCOM-BC) from the
339 ANCOMBC R package (Lin and Peddada, 2020; Nearing *et al.*, 2022). Linear discriminant
340 analysis (LDA) effect size (LefSe) was performed to screen for differentially abundant
341 predicted microbial function (MetaCyc pathways) across the four timepoints , based on an LDA
342 threshold of 2.0 and a statistical significance cut-off of < 0.05 (All-against-all strategy; Segata
343 *et al.*, 2011).

344 Mantel test (Spearman correlation method) was employed to determine the correlation
345 between the *I. nucleus* microbiome taxonomic structure and the oxidized PUFA products using
346 their dissimilarity matrices across timepoints using the mantel() function in vegan package
347 (Oksanen *et al.*, 2022), which tested whether higher dissimilarity in microbiome was associated

348 with higher dissimilarity in metabolite profiles. Since the oysters' microbiome and metabolites
349 were sampled from independent individuals, we averaged each microbial taxon and each
350 metabolite concentration across replicates at each timepoints before generating a dissimilarity
351 distance matrix between samples – Bray-Curtis (microbiome) and Euclidean (metabolites).
352 The GraphPad Prism software (San Diego, California, USA) was used to generate the
353 figure for oyster's body temperatures, individual oxidized PUFA products and the 10 dominant
354 microbe's relative abundance across the timepoints.
355

356 # Results

357 *Tidal dynamics and temporal changes in environmental and body temperatures*

358 Oysters were regularly exposed to the air as a result of the tidal regime (Fig. 1A) and
359 this temporal change was aligned to changes in the rock surface temperature across the day,
360 with the highest temperature recorded at noon (45-50°C, Fig. 1A). The body temperature of the
361 oysters varied temporally within a single emersion period (Fig. 1B; GLM $\mathcal{X}^2_{(3)} = 1073.9$, p-
362 value < 0.05), increasing from 32.11 ± 0.12 °C (mean ± SD) in the morning to 39.99 ± 0.95 °C
363 (mean ± SD) at noon, after which body temperatures drop steadily to ~ 35 °C in the afternoon.
364 Besides early-afternoon (35.4°C ± 0.46) and late-afternoon (35.18 °C ± 0.46), all pairwise
365 comparisons showed significant differences in body temperatures between timepoints.
366

367 *Temporal assessment of oxidized PUFA products*

368 Individual analyses of each oxidized PUFA products revealed that only four products
369 (i.e., 5-F_{2t}-IsoP, 10-F_{4t}-NeuroP, 13-F_{4t}-NeuroP, and 16-F_{1t}-PhytoP) significantly varied
370 between timepoints (Table 1, Fig. 2). These metabolites showed an increased in concentration
371 at noon (10-F_{4t}-NeuroP and 13-F_{4t}-NeuroP) and post-noon (5-F_{2t}-IsoP and 16-F_{1t}-PhytoP)
372 relative to morning, with varying degree in increment among these four metabolites. In
373 particular, 5-F_{2t}-IsoP and 16-F_{1t}-PhytoP exhibited roughly 4-folds increase on average in

374 concentration. There was a significant difference in the metabolite structural profile
375 (PERMANOVA) (contributed by fifteen metabolites) between timepoints (*pseudo-F* = 2.17, p-
376 value < 0.05; Fig. 3A), but PERMDISP indicated no significant difference in their dispersion
377 (F-value = 0.69, p-value > 0.05; Fig. 3A). An additional PERMANOVA analysis with the four
378 temporally-varied products showed a significant difference in the clusters between the morning
379 metabolite profile and all the other timepoints during the emersion period (*pseudo-F* = 5.62, p-
380 value < 0.05; Fig. 3B). Multivariate dispersion of the four oxidized PUFA products also differed
381 between timepoints (F-value = 6.10, p-value < 0.05; Fig. 3B). With the exception of three
382 pairwise comparisons (i.e., noon vs. early-afternoon, noon vs. late-afternoon and early-
383 afternoon vs. late-afternoon), all the other timepoints showed significant differences in
384 dispersion (p < 0.05). Combining both of these results, the metabolite structural profile at the
385 morning timepoint had the smallest dispersion (smaller inter-interindividual difference) when
386 only the four temporally-variable oxidized PUFA products were considered. However, when
387 all products were included in the analysis, the overall group dispersion did not vary across the
388 day.
389
390 *Temporal characterization of oyster-microbiomes*
391 The 16S rRNA amplicon sequencing generated a total of 2,032,567 reads from 30
392 samples which were reduced to 1,126,884 after denoising and quality control. These reads were
393 then used to characterize the microbial communities of *I. nucleus* across the different timepoints.
394 Due to the low sequence counts, samples BRM3 (5612 reads) and DRM4 (7519 reads) were
395 removed after each sample was rarefied to a sampling depth of 21,282 reads.
396 The ASV richness and Shannon-Wiener index of *I. nucleus* microbiome were
397 significantly different between timepoints (ASV richness: $_{3,14)}$ = 3.67; p-value < 0.05; Shannon-
398 Wiener index: $F_{(3,14)}$ = 3.76; p-value < 0.05; Fig. S2). However, no specific temporal trends
399 were detected for all pairwise comparisons in ASV richness. Significant differences were,

400 however, found for the Shannon-Wiener index between morning and noon timepoints. Oyster
401 body temperature significantly influenced ASV richness and Shannon-Wiener indexes,
402 showing an inverse relationship with microbiome alpha diversity (Fig. S3). Overall, morning
403 timepoints showed the highest alpha diversity. This diversity then drastically declined at noon,
404 with partial recovery at the last timepoint – late-afternoon.

405 The top 10 most abundant microbial taxa (at the family level) associated with *I. nucleus*
406 in a descending order were *Mycoplasmataceae, Helicobacteraceae, Spirochaetaceae,*
407 *Xenococcaceae, Rhodobacteceae, Rickettsiales* unknown*, Arcobactericeae, Caldilineaceae,*
408 *Alphaproteobacteria* unknown and *Saprospiraceae* (Fig. 4). These top 10 families made up on
409 average 57.09%, 80.88%, 81.42%, and 68.20% of the overall relative abundance in morning,
410 noon, early-afternoon, and late-afternoon, respectively. Among them, only two families
411 (*Helicobacteraceae* and *Arcobacteraceae*) showed significant differences in the relative
412 abundance between timepoints based on the ANCOM-BC analysis (Fig. S4; *Helicobacteraceae*:
413 morning vs early-afternoon; *Arcobacteraceae*: morning vs noon, and morning vs early-
414 afternoon).

415 LefSe analysis identified 27 differentially abundant microbial functions (MetaCyc
416 pathways; LDA threshold of 2.0) that characterises the microbiome at a particular timepoint
417 (Fig. 5). The most distinctive difference in functions identified were between morning and late-
418 afternoon timepoints, where the former showed a major enrichment in genes associated with
419 biosynthetic pathway (and some biomolecules degradation pathways), while the latter had
420 functions affiliated with degradation, utilization, and assimilation pathways, specifically in
421 carbon metabolism.

422 Assessing the overall microbiome structure in taxonomy and functions with
423 PERMANOVA analysis indicates no significant difference between timepoints (taxonomy:
424 *pseudo-F* = 1.18, p-value > 0.05; function: *pseudo-F* = 1.49, p-value > 0.05 ;Fig. 6), but

significant differences was detected in both of the microbial dispersion profiles (taxonomy: F-value = 3.55, p-value < 0.05; function: F-value = 3.74, p-value < 0.05 ; Fig. 6). Major differences in the taxonomic microbiome dispersion were between morning and early-afternoon, which corresponds to the pre-and post-noon period, respectively. For the functional microbiome, the pair early-afternoon-late-afternoon was the cause of the difference in dispersion. We found no Mantel correlation was observed between the microbiome taxonomic profile and the oxidized PUFA products profile, either with the 15 (all) or 4 metabolite groups (Table 2).

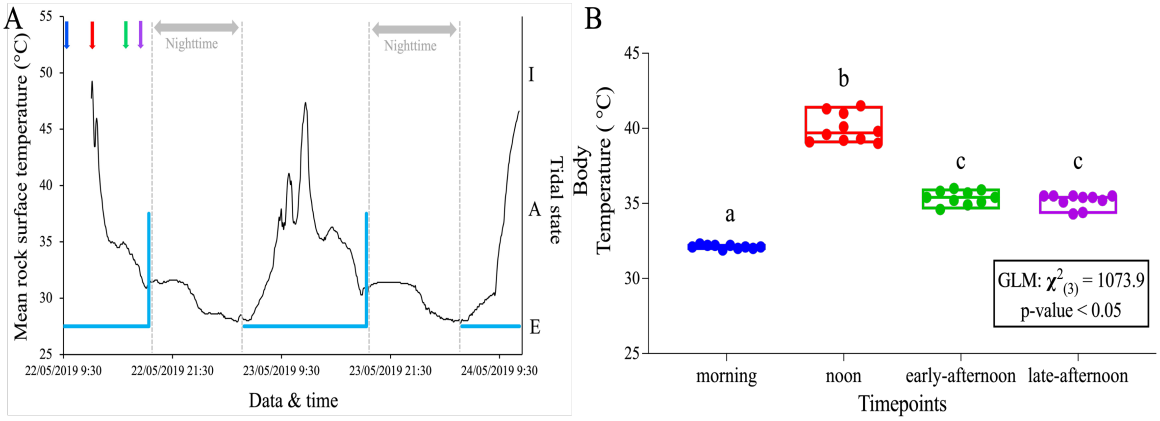

Fig. 1. The body temperature of *Isognomon nucleus* varies across sampling timepoints within a tidal cycle. (A) Thermal (black line) and tidal conditions (blue line) as experienced by *I. nucleus* at the study site. Thermal condition is represented by the mean rock surface temperature (averaged over 3 – 5 i-Button temperature loggers), and tidal condition during the day is categorized into three states: "E" (exposed), "A" (awash), and "I" (immersed). Coloured arrows indicate the sampling time points of *I. nucleus* (colours match to boxplot in Fig. 1B) to assess its physiological responses (i.e., biochemical dynamics) and microbiome taxonomic/functional profile (B) Boxplots showing *I. nucleus* body temperatures (n=10) across different timepoints (Centre line represent the median; box limits indicate the first and third quartiles). Statistical significance (p-value < 0.05) is indicated if the letters above each bar are different.

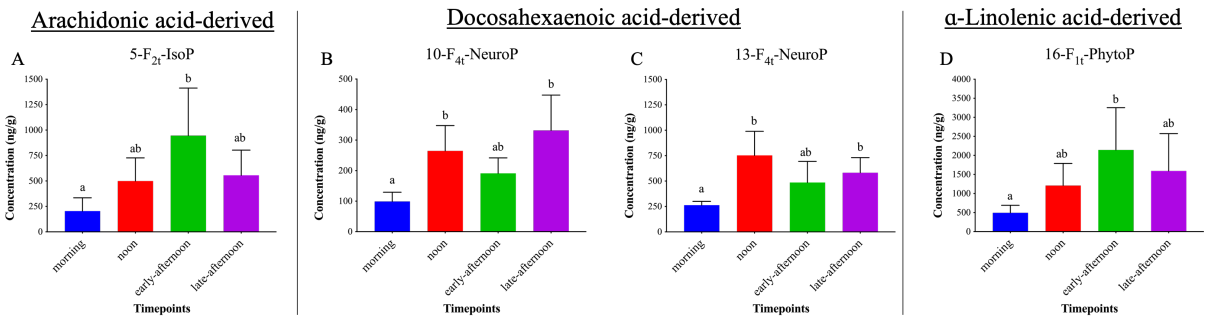

Fig. 2. Four oxidized PUFA products exhibit variation in concentration across the emersion period. Bar graphs showing the four oxidized PUFA products deriving from their respective PUFA (labelled at the top of each panel, across different sampling timepoints in *I. nucleus*. IsoP: isoprostane; NeuroP: 19 europrostane; PhytoP: phytoprostanes. Data are presented as mean concentration and + 1 standard deviation (error bar) for each metabolite (n=5) at the given timepoints. Statistical significance (p-value < 0.05) is indicated if the letters above each bar are different.

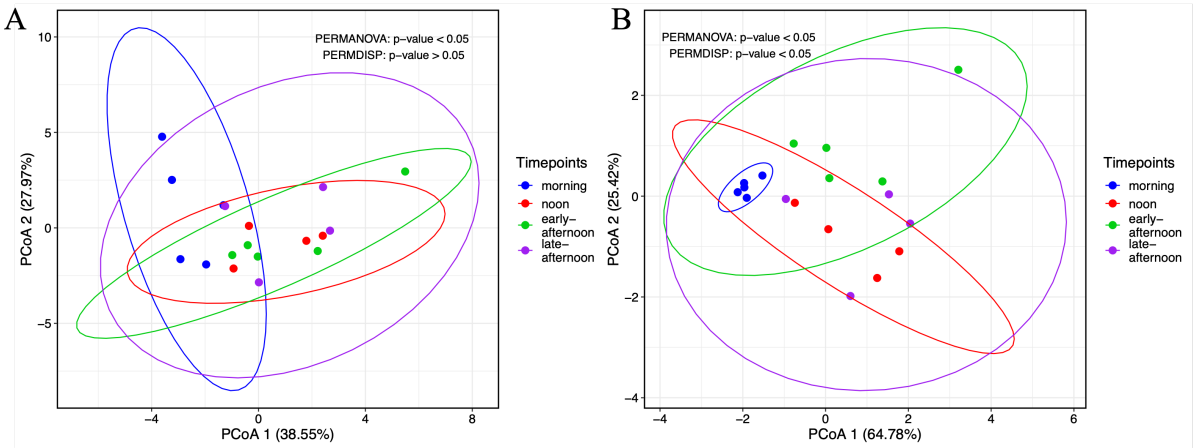

Fig. 3. Oxidized PUFA products profile varies across the emersion period. PCoA based on Euclidean distance measured between samples from different timepoints based on (A) all oxidized PUFA products (B) four oxidized PUFA products: 5-F_{2t}-IsoP, 10-F_{4t}-NeuroP, 13-F_{4t}-NeuroP, and 16-F_{1t}-PhytoP. The colours of the datapoints and ellipses (95% confidence interval of the true multivariate means) indicate their corresponding timepoints.

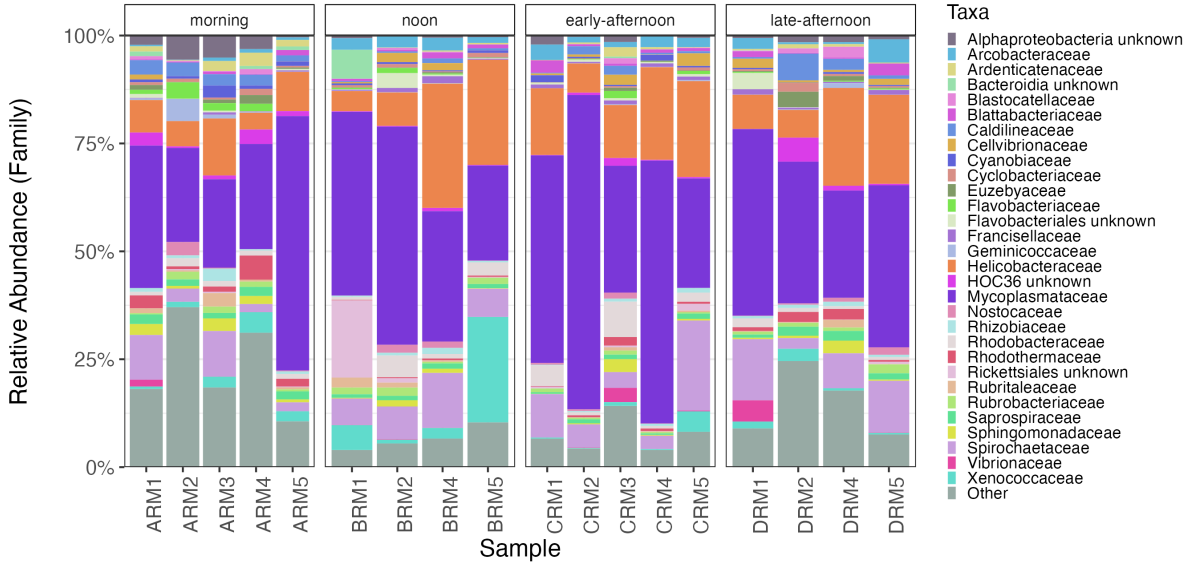

Fig. 4. Relative abundance of top 30 most dominant microbial taxa associated with the *I. nucleus's* gut microbiome at each sampling timepoints. ASV counts were aggregated into the family taxonomic level. Each bar represents a single individual replicate of oyster gut microbiome.

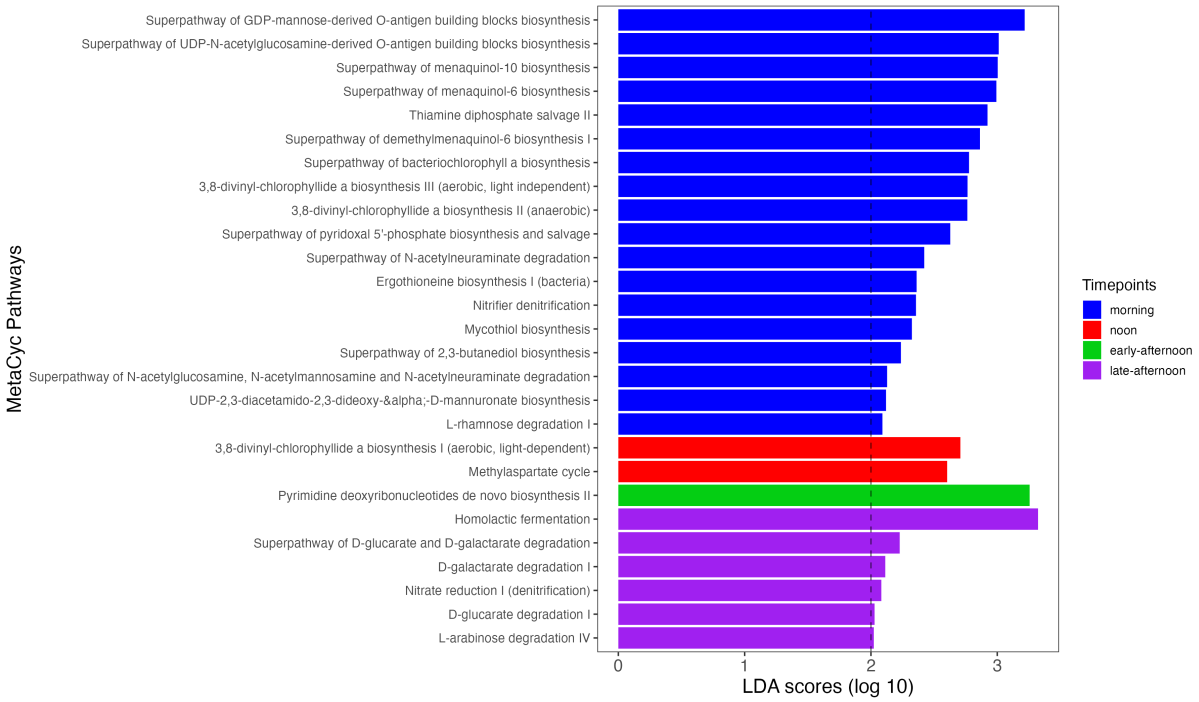

Fig. 5. Differentially abundant microbial functions associated with a particular time point. LefSe analysis (LDA scores of > 2 and alpha of 0.05) showing 27 predicted functions (MetaCyc) pathways) that was identified as discriminative among the timepoints. Coloured bar represents functions that was derived from a particular timepoint. The LDA scores cut-off is depicted by the dotted lines.

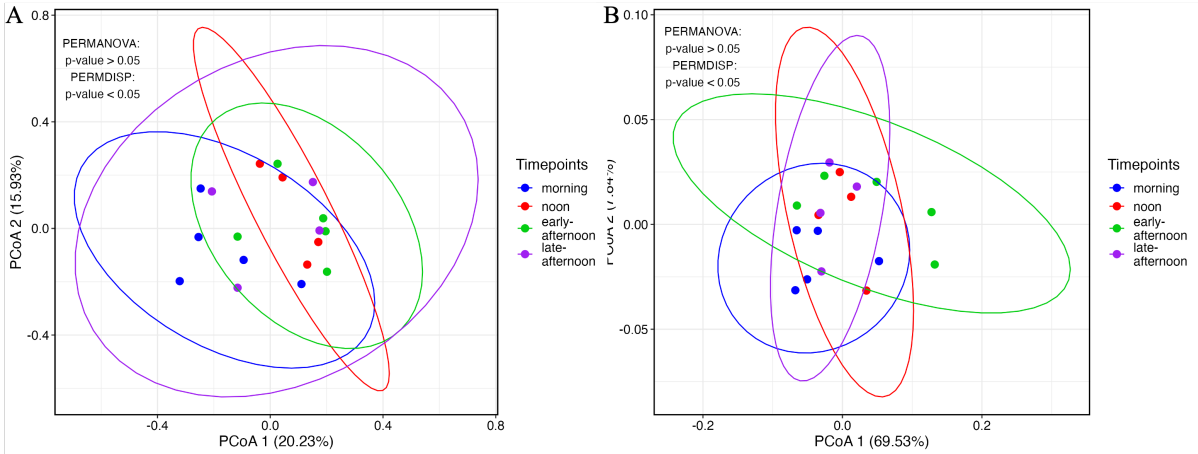

Fig. 6. *I. nucleus*-associated microbiome taxonomic and functional structures exhibit variation in dispersion across the emersion period. PCoA based on the Bray-Curtis distance metric measured between samples from different timepoints, based on (A) taxonomy (ASV level) and (B) functions (MetaCyc pathways). The colours of the datapoints and ellipses (95% confidence interval of the true multivariate means) indicate their corresponding timepoints.

Table 1. Statistical analysis result (ANOVA or GLM with gamma distribution) testing the effect of timepoints on the concentration of each of the oxidized PUFA products.

PUFA	Metabolite	Test Statistic	p-value
Arachidonic acid	5-F_{2t}-IsoP	$F_{(3,14)} = 5.08$	**0.04**
	15-F_{2t}-IsoP	$F_{(3,14)} = 1.72$	0.21
Adrenic acid	7-F_{2t}-Dihomo-IsoP	$F_{(3,14)} = 3.10$	0.06
	17-F_{2t}-Dihomo-IsoP	GLM $\mathcal{X}^2_{(3)} = 0.66$	0.69
Docosahexaenoic acid	4-F_{4t}-NeuroP	$F_{(3,14)} = 3.13$	0.06
	10-F_{4t}-NeuroP	$F_{(3,14)} = 8.43$	**< 0.01**
	13-F_{4t}-NeuroP	GLM $\mathcal{X}^2_{(3)} = 27.46$	**< 0.01**
	20-F_{4t}-NeuroP	$F_{(3,14)} = 1.23$	0.34
α-Linolenic acid	9-D_{1t}-PhytoP	$F_{(3,14)} = 0.58$	0.64
	9-F_{1t}-PhytoP	GLM $\mathcal{X}^2_{(3)} = 7.92$	0.05
	16-F_{1t}-PhytoP	$F_{(3,14)} = 3.72$	**0.04**
	16-B_{1t}-PhytoP	GLM $\mathcal{X}^2_{(3)} = 6.66$	0.08
Eicosapentaenoic acid	5-F_{3t}-IsoP	$F_{(3,14)} = 2.49$	0.10
	15-F_{3t}-IsoP	GLM $\mathcal{X}^2_{(3)} = 0.32$	0.32
	8-F_{3t}-IsoP	$F_{(3,14)} = 0.81$	0.51

491 **Table 2**. Mantel's spearman's rank correlation I and p-value to investigate the association
492 between the *I. nucleus* microbiome taxonomic structure (mean abundance of each taxon across
493 all timepoints) and oxidized PUFA products profile (mean concentration across timepoints).
494 The number of permutations performed was 23(maximum possible).
495

Association with microbiome taxonomic structure	Mantel's r	p-value
oxidized PUFA products (all)	0.77	0.21
oxidized PUFA products (Four)*	0.54	0.25

496 *The four metabolites were: 5-F_{2t}-IsoP, 10-F_{4t}-NeuroP, 13-F_{4t}-NeuroP, and 16-F_{1t}-PhytoP

497

498 # Discussion

499 Organisms living on the intertidal rocky shore regularly experience drastic changes in
500 environmental temperature (Somero, 2002; Stillman, 2002; Harley, 2008). For many sessile
501 ectotherms, this represents a physiological challenge due to their inability to escape from heat
502 stress (e.g. seeking thermal refuge) and so, they rely on various intrinsic (e.g., metabolic and
503 physiological plasticity) and extrinsic (e.g., host-associated microbiome; still underexplored)
504 mechanisms to cope with temperature fluctuations (Lathlean *et al.*, 2014; Giomi *et al.*, 2016;
505 Bang *et al.*, 2018). As with other ectotherms, the body temperature of the high-supratidal oyster
506 *Isognomon nucleus*, was highly influenced by changes in ambient temperature, emersion, and
507 the reduction in oxygen availability and food during the low-tide period. Such changes
508 particularly in temperature, are known to induce physiological stress and metabolic depression
509 (Hui *et al.*, 2020), with the associated oxidative stress (Hermes-Lima *et al.*, 2015). Here, linked
510 to these physiological conditions, we found adjustments in four major non-enzymatic oxidized
511 PUFA products (i.e., 5-F_{2t}-IsoP, 10-F_{4t}-NeuroP, 13-F_{4t}-NeuroP, and 16-F_{1t}-PhytoP) that reflect
512 temporal variation in the oxidative stress experienced by the oysters. When assessing the
513 microbiome profile through time, there was a significant change in the alpha diversity,
514 dominant microbial and specific functional enrichment. No clear temporal change in beta-
515 diversity was detected in the gut microbiome, despite the significant variation in group

516 dispersion. Our study found a lack of temporal correlation between the intrinsic (biochemical
517 profile) and extrinsic (microbiome taxonomic structure) mechanisms studied. These findings
518 suggest that environmental variation and/or host thermal condition (within a single emersion
519 period), can drive independent physiological responses (biochemistry – oxidized PUFA
520 products) and temporal dynamics in the gut microbiome of the tropical intertidal oyster *I.*
521 *nucleus*. These independent responses may be important for the overall homeostasis of the
522 oysters, and their ability to cope and survive in the thermally challenging tropical high-
523 supratidal environment. However, manipulative experiments would be needed to confirm this
524 hypothesis.
525

526 *The intrinsic mechanism underpinning oysters' adaptive response to temporal*
527 *environmental changes*

528 For high-supratidal zone inhabiting ectotherms, metabolic depression is an adaptive
529 response that allows them to cope with extreme high and stressful thermal conditions (Sokolova
530 and Pörtner, 2001; Marshall *et al.*, 2011). In a laboratory setting, Hui et al. (2020) demonstrated
531 that the oyster *I. nucleus* consistently enters into metabolic depression (i.e., measured by heart
532 rate) when body temperature approaches ~ 37°C (a value that is regularly surpassed on daily
533 basis at around noon on tropical rocky shores). Based on this previous study, our data indicates
534 that the oysters could have entered a state of metabolic depression when exposed during the
535 low tide at noon time (*I. nucleus* noon temperature: ~ 39.99 ± 0.95 ℃). After this, oysters
536 resumed their metabolic activity when body temperatures decreased (i.e., late
537 afternoon/evening).

538 Intertidal bivalves are known to also display intermittent gaping behaviour during
539 periods of aerial exposure as a way to enhance oxygen intake and evaporative cooling,
540 particularly when experiencing thermal stress (Lent, 1969; Mcmahon, 1988; Nicastro *et al.*,

541 2010). In our study, all individuals shut their valves and no intermittent gaping behaviour was
542 observed either during the high thermal stress or the recovering period (Hui, T.Y., unpublished
543 data). Therefore, these oysters are expected to experience low oxygen availability within the
544 shells, if not hypoxia. Under such condition, metabolic depression is a critical strategy for
545 survival, reducing energy consumption and the elevation of ROS. This strategy is particularly
546 relevant at noon where these oysters experienced the highest environmental temperature, which
547 is usually associated with an increase in metabolic demand (Hermes-Lima *et al.*, 2015; Jiang *et*
548 *al.*, 2020; Wang *et al.*, 2022).

549 There were four metabolites (i.e., 5-F_{2t}-IsoP (Isoprostane), 10-F_{4t}-NeuroP
550 (Neuroprostane), 13-F_{4t}-NeuroP (Neuroprostane), and 16-F_{1t}-PhytoP (Phytoprostane)) that
551 showed visible temporal patterns, potentially associated with their metabolic regulation. Such
552 patterns may be linked to the sensitivity of the metabolites to ROS changes in the oyster. The
553 elevation of two metabolites at noon (10-F_{4t}-NeuroP and 13-F_{4t}-NeuroP) and two metabolites
554 (5-F_{2t}-IsoP, and 16-F_{1t}-PhytoP) at post-noon timepoints, clearly indicates that oysters
555 experienced a rise in the ROS level, a signal of oxidative stress (Hermes-Lima and Zenteno-
556 Savín, 2002; Storey and Storey, 2004; Welker *et al.*, 2013; Galano *et al.*, 2017). The high levels
557 of 16-F_{1t}-PhytoP (Phytoprostane) metabolites, compared to other three oxidized PUFA
558 products in the *I. nucleus,* imply that the PUFA ALA could be the primary target for lipid
559 oxidative damage in this oyster. Our findings (i.e., changes in these metabolites over a short
560 period of time ~3 hours: morning – noon), support the observations by Williams and Somero
561 (1996). These authors showed that over a short period of time (within hours), the gills of the
562 intertidal *mussels Mytilus califonianus* (high intertidal zone) exhibit an alteration in the cellular
563 membrane order/fluidity (i.e., phospholipid vesicles), in response to thermal variation
564 encountered during a single period of tidal cycle. Thus, the rapid alteration in the biochemical
565 profile observed in our study could be an important response for the survival of the oysters

566 during periods of thermal stress and fluctuations in the intertidal rocky shore.

567 Further analysis with the overall structural profile with the four ROS-sensitive oxidized
568 PUFA products showed a clear temporal variation and inter-individual variation in *I. nucleus*.
569 The large inter-individual variation in the oxidized PUFA products profile at noon/afternoon
570 relative to morning timepoint might be related to the thermal and oxidative stress conditions
571 experienced by the oysters during those periods of elevated temperatures. This variability
572 suggests inter-individual differences in physiological plasticity, regulation, and sensitivities to
573 environmental stress. The result here also indicates that the polyunsaturated fatty acids (ARA,
574 DHA, and ALA) from which these four oxidized PUFA products were derived, may play a key
575 role as lipid metabolites that help to resolve inflammation and oxidative stress for the oysters
576 to return to homeostasis (Roy *et al.*, 2017; Lee *et al.*, 2020). It is important to highlight here
577 that the current understanding regarding the thermal-physiological roles of high PUFA ALA or
578 the oxidized PUFA products in *I. nucleus* is still limited and that our interpretations are
579 speculative and idiosyncratic to the specific animals and population studied. Moreover, our
580 assessment was based on the observation and analysis that are known in clinical research and
581 we remained carefully and strictly conservative in our discussion to just focus on the association
582 between these products and the host oxidative stress level. Future studies would be dedicated
583 toward elucidating the role of these molecules that may be essential to their host physiology
584 and metabolism.

585

586 *The extrinsic mechanism underpinning the oysters' response to temporal*
587 *environmental changes*

588 Host-associated microbiome diversity, structure, and functions are considered as
589 important components of animal adaptation and acclimation to environmental change (Foster
590 *et al.*, 2017; Bang *et al.*, 2018; Voolstra and Ziegler, 2020). Alterations in microbiome diversity
591 can be associated with the direct influence of the host's physiology and/or with host-

592 independent environmental effects (Shiu *et al.*, 2017; Li *et al.*, 2018, 2022; Muñoz *et al.*, 2019).
593 In our study, the composition and diversity (ASV richness and Shannon diversity) of the oyster
594 gut-associated microbiome varied with time which coincided with variation in the oyster's
595 body temperature, suggesting that the thermal condition experienced by the host may modulate
596 the microbial alpha diversity via either direct/indirect physio-biochemical influences (Sorek *et*
597 *al.*, 2014; Pita *et al.*, 2018; Liu *et al.*, 2023). In the morning, the oyster's gut had a significantly
598 more diverse microbiome diversity, which may be linked to the less thermally stressed host
599 (Hui *et al.*, 2020), and/or to the filter-feeding activities before being exposed by the receding
600 tide (Parris *et al.*, 2019). However, based on the Shannon alpha diversity, at early post-noon
601 condition, a major decline in diversity was observed, which may be associated with the thermal
602 physiological stress experienced by the host (body temperature is within the metabolic
603 depression range; Hui *et al.*, 2020) and oxidative stress (indicated by the rise in the two oxidized
604 PUFA products at noon and two at early post-noon condition). This decline in diversity is also
605 a common pattern seen in many marine organisms under physiological stress (Green and Barnes,
606 2010; Li *et al.*, 2018; Hartman *et al.*, 2020). For example, Lokmer & Wegner (2015) showed
607 that acute thermal stress and/or infection caused a marked decline in the alpha diversity of the
608 microbiome in the oyster *Crassostrea gigas*. In another study by Li et al. (2018) observed an
609 overall decrease in the gut microbial alpha diversity associated with the mussel, *Mytilus*
610 *coruscus*, after exposing to higher temperature. Such observation offer support to our result
611 where the relatively higher temperature at noon may have driven the decline in the oyster-
612 associated microbial diversity.

613 Whilst the temporal changes exhibited by the *I. nucleus* microbiome and their
614 association with changes in the oysters' body temperatures suggest that the microbiome
615 composition may be actively regulated by the host, differential sensitivities of certain bacterial
616 taxa to external environmental changes may also be an important mechanism driving the

temporal variation in the microbiome composition. *Arcobacteraceae* and *Helicobacteraceae* are the only two dominant family-level microbial taxa associated with the temporal thermal/oxidative stress variation of the host. In particular, there was an elevated relative abundance of these two bacteria groups at noon and/or at the afternoon timepoints, which may suggest that their abundances during these periods were promoted by specific host/environmental conditions, facilitating their growth probably by reducing competition (Garren *et al.*, 2016; Shaver *et al.*, 2017; Sharp and Foster, 2022). *Arcobacteraceae* is a group of common opportunistic bacteria found in marine bivalves and is known to be associated with disease-causing bacteria such as *Vibrio* (Lokmer and Wegner, 2015; de Lorgeril *et al.*, 2018). In many studies, the elevation of the *Arcobacteraceae* has been associated with the thermal stress condition experienced by the host (Lokmer and Wegner, 2015; Shiu *et al.*, 2017; Neu *et al.*, 2021). Members of *Arcobacteraceae* are also known to be microaerophilic as they tend to grow better under a low-oxygen environment (Vandamme and De Ley, 1991). This may explain the dominant presence of *Arcobacteraceae* within the oysters' microbiome due to the prevailing hypoxic and thermally stressful conditions as experienced by the oyster hosts during emersion. Similarly, the presence and abundance *Helicobacteraceae* can be associated to oxygen levels in the marine environment. For instance, certain members of this family are capable of oxidising sulfide, and thus, they might contribute with a detoxification function to the oyster host (Kodama and Watanabe, 2004; Nakagawa *et al.*, 2017; Neu *et al.*, 2021). The accumulation of sulfide can be detrimental or lethal to marine bivalves (Le Moullac *et al.*, 2008), and it is typically associated with hypoxic stress (Le Moullac *et al.*, 2008; Pal *et al.*, 2018). Such stress is hypothesised to occur in *I. nucleus* during aerial exposure, as no intermittent gaping behaviour was detected. When oxygen is low, sulfide production is promoted by the activity of hydrogen sulfide-producing bacteria such as *Desulfobacterota* members (Flannigan *et al.*, 2011; present in the I. nucleus; Dordević *et al.*, 2021; Pimentel *et al.*, 2021). It is unclear, however,

642 the extent to which the dynamics in the abundance of sulfide-producing bacteria and
643 *Helicobacteraceae* members (with potential detoxification role), are functionally
644 interconnected. While this seems likely, we are unaware of any study exploring this functional
645 link, and it would be important to investigate such species' interaction and its effects on the
646 physiology and fitness of the host.

647 Variation in the microbiome functional activity is commonly associated with the
648 functional changes occurring within the host (e.g., dietary changes; Mekuchi *et al.*, 2018;
649 Masasa *et al.*, 2023) and/or in the external environment (e.g., temperature; Brothers *et al.*, 2018;
650 Li *et al.*, 2022). Our study is in-line with this, in showing that there were several enriched
651 functions that vary through time, potentially attributed to either one or both of those two factors.
652 Specifically, in the morning timepoints, we detected a major proportion of predicted
653 microbiome function in biosynthetic pathways associated with carbohydrate, cofactor, carrier,
654 vitamin and secondary metabolites biosynthesis. This suggested that, in the morning, the host
655 gut had a considerable dietary resources for the building of these organic/inorganic molecules
656 in microbes to support cellular maintenance and growth and/or actively contributing to host
657 nutritional metabolism (David *et al.*, 2014; Maurice *et al.*, 2015; Dubé *et al.*, 2019). On contrary,
658 post-noon conditions were significantly dominated by compound/molecular degradation
659 pathways associated with carbon metabolism. This makes sense since in the post-noon
660 conditions (post-heat stress), the host are likely in a "recovery" that could incur a high energetic
661 requirement for various cellular and physiological repair and maintenance purposes (Storey and
662 Storey, 2004; Sokolova *et al.*, 2011). The breakdown of these carbon compounds by the
663 microbes can provide as an energy source to meeting the metabolic demand in the host and
664 microbes (Flint *et al.*, 2012; Tremaroli and Bäckhed, 2012; Den Besten *et al.*, 2013). However,
665 it is unclear if these predicted microbial functional enrichments are directly contributing to the
666 host dietary metabolism (e..g., nutrient absorption; English *et al.*, 2023) or simply fulfilment of

667 need for the microbes themselves (host-independent) to cope and survive to the prevailing
668 conditions (i.e., host and/or external environmental influence).

669 Host tolerance and resilience to environmental stress are known to be conditioned by
670 the stability/flexibility of its associated microbiome. While we found no major differences in
671 microbiome beta diversity throughout the emersion period (based on PERMANOVA), there
672 was a significant difference in dispersion between the timepoints. This suggests that the
673 temporal change in the environment and host could influence the inter-individual variation in
674 their microbial profile. Such temporal differences (particularly in alpha diversity) could
675 potentially be explained by the ability of the host to control/regulate the microbiome during a
676 disturbance event (Sharp *et al.*, 2017; Pita *et al.*, 2018; Rocca *et al.*, 2019; Rädecker *et al.*,
677 2022). Alternatively, temporal changes in the microbiome may reflect the result of its own
678 control in response to changing and stressful environments, rather than the host
679 control/regulation (Soen, 2014). These findings contrast with other studies showing that
680 microbiome stability is essential for host tolerance and acclimation to environmental challenges
681 such as thermal stress. For example, Santoro et al. (2021) demonstrated that the stability of
682 inoculated "beneficial microorganisms" in the coral *Mussismilia hispida* provided a thermal
683 protection effect, reducing heat stress and preventing the associated mortality (40% increase in
684 the survival rate) of the hosts. Regardless whether it is host control or an independent reultation
685 of the microbiome, the resilience of this extrinsic mechanism may contribute to the survival of
686 *I. nucleus* in the thermally extreme tropical intertidal environment (Bang *et al.*, 2018; Aktipis
687 and Beltran, 2021).

688 *No correlation between microbiome structure and oxidized PUFA products*
689 *profile*

690 Over the decades, many studies have documented the role and action of PUFA (e.g., as
691 probiotics) in modulating dynamics in the gut microbiome of different animals (Huyben *et al.*,
692 2020; Fu *et al.*, 2021; Lau *et al.*, 2022; Ma *et al.*, 2022). Hence, it is expected that stress-driven

693 changes in these biochemicals and their by-products would influence the oyster gut microbiome.
694 However, we found no correlation between the oxidized PUFA products (averaged across all
695 tissues) and the gut microbiome taxonomic structure in *I. nucleus*, despite the temporal and
696 inter-individual variation in the oxidized PUFA products profile across the emersion period.
697 The lack of association between the microbial and oxidized PUFA products profiles of *I.*
698 *nucleus*, suggests two possibilities that are not mutually exclusive. Firstly, as mentioned
699 previously, physiological/biochemical and microbiome profiles may have different sensitivities
700 to changes in environmental conditions. Secondly, such microbiome profiles and biochemical
701 responses may not show strong variation and/or alignment because of local adaptation. Here,
702 the thermal window and oxygen levels experienced by the oysters, although extreme for many
703 ectotherms, can be considered within the tolerance range of the species. Several studies have
704 shown that the microbiome-metabolites correlation is detectable only under severe post-
705 disturbance events and unhealthy host conditions (Nguyen *et al.*, 2021; Pimentel *et al.*, 2021;
706 Walke *et al.*, 2021; Mallott *et al.*, 2022), which go beyond tolerance levels. Thus, in this study,
707 oysters may be in a condition where stress is within the tolerance range, and thus no correlation
708 can be observed between these two components (i.e., host biochemical profile and microbiome
709 structure). Future studies aiming to explore the functional regulation and interplay between
710 intrinsic and extrinsic mechanisms in ectotherms living in the thermally extreme and fluctuating
711 environment like in this study, the intertidal rocky shore, require the assessment of both
712 components when animals are closer to, or surpass their physiological tolerance limits at
713 sublethal levels.

714 *Study limitations*
715
716 While our findings are noteworthy, here we discuss some study limitations and potential
717 recommendations to address them. First, temperature-modulated dynamics in host-associated
718 microbial communities and biochemical profiles across the day lacked temporal replication.
719 Although the selected timepoints are eco-physiologically relevant for the oysters, the
720 consistency and repeatability of the trends observed can only be assessed by sampling at
721 different and independent days (i.e., two or more non-consecutive days). Second, the timepoints
722 selected, although extreme for most ectotherms on Earth, fell within a thermal window that
723 represents acute low physiological stress to the oysters. Major and divergent differences in
724 extrinsic and intrinsic responses might potentially be detected under acute high or chronic
725 physiological stress when body temperatures reach the maximum temperature documented for
726 this species 50-52ºC in the field (Fig. 1). Third, the existence of an interacting drivers that may
727 influence the microbiome altogether, such as, temperature, hypoxic condition (no gaping in the
728 oyster) and the emersion duration. This makes our study difficult to distinguish the influence
729 of a sole driver in the field. Fourth, the oyster microbiome can exhibit tissue-specific profiles
730 associated to functional differences (Dubé *et al.*, 2019). Here, our focus was the gut microbiome
731 as its captures a large diverse microbial sets associated with their host (King *et al.*, 2012; Pierce
732 and Ward, 2018; Dubé *et al.*, 2019), and several documented findings showing their strong and
733 direct signal of their host physiological states (Li *et al.*, 2018; Pierce and Evan, 2019; Fassarella
734 *et al.*, 2021; Stevick *et al.*, 2021). However, other tissues such as the haemolymph or the gills
735 of the oysters can provide complementary information regarding the interaction between
736 microbial communities and their host under environmental stress (Lokmer and Wegner, 2015;
737 Scanes *et al.*, 2021). Despite these limitations, our study provides for the first-time empirical
738 evidence of the intrinsic and extrinsic mechanisms underpinning the temperature tolerances and
739 ecological success of tropical high-supratidal zone inhabiting ectotherms. Future studies can

integrate our recommendations to provide more robust and independent assessments of temporal dynamics in temperature-modulated functional responses of ectotherms in extreme environments.

Conclusion

Intrinsic (i.e., non-enzymatic oxidized PUFA products) and extrinsic (i.e., microbiome) mechanisms linked to the ecophysiology and tolerance/sensitivity of the oyster *Isognomon nucleus*, showed temporal variation, indicative of thermal and oxidative stress. Such trend showed a temporal association with the environmental and body temperatures during the tidal cycle where oysters were fully emersed. We observed a dynamic pattern in the oyster's gut microbiome in terms of the alpha diversity, specific individual microbial taxa and functions that varied along this temporal and environmental cycle. However, limited changes were detected in the overall structure and function of the associated microbial communities. When assessing both the intrinsic and extrinsic mechanisms together, we found no clear correlation between the oxidized PUFA products profile and the microbiome profile, suggesting an independent influence from the environment and/or the host thermal condition on these two profiles. To our best knowledge, this is the first study to report the use of non-enzymatic oxidized PUFA products as a proxy for oxidative stress levels in intertidal animals and profiling short-term dynamics of the host-associated microbiome in an intertidal environment. Future investigations should aim to explore the interplay between these biomolecules and microbial patterns when stressful environmental conditions are unpredictable and beyond tolerance windows of the hosts. Moreover, it is important to understand whether these functional links between intrinsic and extrinsic mechanisms are modulated by local adaptation and can be shared among other intertidal organisms.

Competing interests

The authors declare no competing or financial interests

Author Contributions

JDGE and BSA conceived the idea and designed the work. BSA carried out most of the work: data collection, sample processing, statistical analyses, and data presentation. AWTC, HTY GAW, and MG were involved in sample and environmental data collection. LKS performed the oxidized PUFA products extraction and processing. TD supplied the in-house synthesised oxidized lipids standards for PUFA metabolites quantification. JTY and TD were involved in analysing the metabolite data. BSA led the manuscript writing with continuous feedback from JDGE. All authors provided feedback on the final version of this work, and accepted responsibility for the entire content of this manuscript.

Acknowledgement

We would like to thank The Swire Group of Companies, especially Ms. Tina Chan and Cathay Pacific staff for arranging air transportation of equipment to and from Thailand from Hong Kong

Funding

BA and JDGE were supported by the Research Grants Council (GRF 17113221) of Hong Kong.

Data availability

All raw data, and scripts will be made available once published.

References

Ahmed, H.I., Herrera, M., Liew, Y.J., and Aranda, M. (2019) Long-term temperature stress in the coral model Aiptasia supports the "Anna Karenina Principle" for bacterial microbiomes. *Front Microbiol* **10**: 975.

Aktipis, A. and Beltran, D.G. (2021) Can some microbes promote host stress and benefit evolutionarily from this strategy? *BioEssays* **43**: 1–11.

Alberdi, A., Aizpurua, O., Bohmann, K., Zepeda-Mendoza, M.L., and Gilbert, M.T.P. (2016) Do vertebrate gut metagenomes confer rapid ecological adaptation? *Trends Ecol Evol* **31**: 689–699.

Apprill, A. (2017) Marine animal microbiomes: Toward understanding host-microbiome interactions in a changing ocean. *Front Mar Sci* **4**: 222.

Bang, C., Dagan, T., Deines, P., Dubilier, N., Duschl, W.J., Fraune, S., et al. (2018) Metaorganisms in extreme environments: do microbes play a role in organismal adaptation? *Zoology* **127**: 1–19.

Basu, S. (2010) Fatty acid oxidation and isoprostanes: Oxidative strain and oxidative stress. *Prostaglandins Leukot Essent Fat Acids* **82**: 219–225.

van den Berg, R.A., Hoefsloot, H.C.J., Westerhuis, J.A., Smilde, A.K., and van der Werf, M.J. (2006) Centering, scaling, and transformations: Improving the biological information content of metabolomics data. *BMC Genomics* **7**: 1–15.

Den Besten, G., Van Eunen, K., Groen, A.K., Venema, K., Reijngoud, D.J., and Bakker, B.M. (2013) The role of short-chain fatty acids in the interplay between diet, gut microbiota, and host energy metabolism. *J Lipid Res* **54**: 2325–2340.

Birben, E., Sahiner, U.M., Sackesen, C., Erzurum, S., and Kalayci, O. (2012) Oxidative stress and antioxidant defense. *World Allergy Organ J* **5**: 9–19.

Bolyen, E., Rideout, J.R., Dillon, M.R., Bokulich, N.A., Abnet, C.C., Al-Ghalith, G.A., et al. (2019) Reproducible, interactive, scalable and extensible microbiome data science using QIIME 2. *Nat Biotechnol* **37**: 852–857.

Brothers, C.J., Pol, W.J. Van Der, Morrow, C.D., Hakim, J.A., Koo, Hyunmin, Mcclintock, J.B., et al. (2018) Ocean warming alters predicted microbiome functionality in a common sea urchin. *Proc R Soc B Biol Sci* **285**:.

Callahan, B.J., McMurdie, P.J., and Holmes, S.P. (2017) Exact sequence variants should replace operational taxonomic units in marker-gene data analysis. *ISME J* **11**: 2639–2643.

Callahan, B.J., McMurdie, P.J., Rosen, M.J., Han, A.W., Johnson, A.J.A., and Holmes, S.P. (2016) DADA2: High-resolution sample inference from Illumina amplicon data. *Nat Methods* **13**: 581–583.

Carey, H. V. and Duddleston, K.N. (2014) Animal-microbial symbioses in changing environments. *J Therm Biol* **44**: 78–84.

Chow, C.Y. (2004) Foraging behaviour of Thais clavigera: The interplay of environmental variation and predator behaviour on sheltered rocky shores.

David, L.A., Maurice, C.F., Carmody, R.N., Gootenberg, D.B., Button, J.E., Wolfe, B.E., et al. (2014) Diet rapidly and reproducibly alters the human gut microbiome. *Nature* **505**: 559–563.

Díaz-Almeyda, E.M., Ryba, T., Ohdera, A.H., Collins, S.M., Shafer, N., Link, C., et al. (2022) Thermal stress has minimal effects on bacterial communities of thermotolerant *Symbiodinium* cultures. *Front Ecol Evol* **10**: 764086.

Dordević, D., Jančíková, S., Vítězová, M., and Kushkevych, I. (2021) Hydrogen sulfide toxicity in the gut environment: Meta-analysis of sulfate-reducing and lactic acid bacteria in inflammatory processes. *J Adv Res* **27**: 55–69.

Douglas, G.M., Maffei, V.J., Zaneveld, J.R., Yurgel, S.N., Brown, J.R., Taylor, C.M., et al. (2020) PICRUSt2 for prediction of metagenome functions. *Nat Biotechnol* **38**: 669–673.

Dubé, C.E., Ky, C.L., and Planes, S. (2019) Microbiome of the black-lipped pearl oyster *Pinctada margaritifera*, a multi-tissue description with functional profiling. *Front Microbiol* **10**: 1548.

Dupuy, A., Le Faouder, P., Vigor, C., Oger, C., Galano, J.M., Dray, C., et al. (2016) Simultaneous quantitative profiling of 20 isoprostanoids from omega-3 and omega-6 polyunsaturated fatty acids by LC-MS/MS in various biological samples. *Anal Chim Acta* **921**: 46–58.

Durand, T., Bultel-Poncé, V., Guy, A., Berger, S., Mueller, M.J., and Galano, J.M. (2009) New bioactive oxylipins formed by non-enzymatic free-radical-catalyzed pathways: The phytoprostanes. *Lipids* **44**: 875–888.

English, M.K., Langdon, C.J., Schubiger, C.B., and Mueller, R.S. (2023) Dominant bacterial taxa drive microbiome differences of juvenile Pacific oysters of the same age and variable sizes. 1–12.

Epstein, H.E., Torda, G., and van Oppen, M.J.H. (2019) Relative stability of the *Pocillopora acuta* microbiome throughout a thermal stress event. *Coral Reefs* **38**: 373–386.

Fadhlaoui, M. and Lavoie, I. (2021) Effects of temperature and glyphosate on fatty acid composition, antioxidant capacity, and lipid peroxidation in the gastropod lymneae sp. *Water (Switzerland)* **13**:.

Fan, L., Liu, M., Simister, R., Webster, N.S., and Thomas, T. (2013) Marine microbial symbiosis heats up: the phylogenetic and functional response of a sponge holobiont to thermal stress. *ISME J* **7**: 991–1002.

Fassarella, M., Blaak, E.E., Penders, J., Nauta, A., Smidt, H., and Zoetendal, E.G. (2021) Gut microbiome stability and resilience: Elucidating the response to perturbations in order to modulate gut health. *Gut* **70**: 595–605.

Feng, J., Zhang, L., Tang, X., Xia, X., Hu, W., and Zhou, P. (2021) Season and geography induced variation in sea cucumber (*Stichopus japonicus*) nutritional composition and gut microbiota. *J Food Compos Anal* **101**: 103838.

Flannigan, K.L., McCoy, K.D., and Wallace, J.L. (2011) Eukaryotic and prokaryotic contributions to colonic hydrogen sulfide synthesis. *Am J Physiol - Gastrointest Liver Physiol* **301**: 188–193.

Flint, H.J., Scott, K.P., Duncan, S.H., Louis, P., and Forano, E. (2012) Microbial degradation of complex carbohydrates in the gut. *Gut Microbes* **3**:.

Folch, J., Lees, M., and Sloane Stanley, G.H. (1957) A simple method for the isolation and purification of total lipides from animal tissues. *J Biol Chem* **226**: 497–509.

Fontaine, S.S. and Kohl, K.D. (2023) The microbiome buffers tadpole hosts from heat stress : a hologenomic approach to understand host-microbe interactions under warming. *J ofp Exp Biol* **226**:.

Fontaine, S.S., Mineo, P.M., and Kohl, K.D. (2022) Experimental manipulation of microbiota reduces host thermal tolerance and fitness under heat stress in a vertebrate ectotherm. *Nat Ecol Evol* **6**: 405–417.

Foster, K.R., Schluter, J., Coyte, K.Z., and Rakoff-Nahoum, S. (2017) The evolution of the host microbiome as an ecosystem on a leash. *Nature* **548**: 43–51.

Fox, J. and Weisberg, S. (2019) An R Companion to Applied Regression.

Freire, C.A., Welker, A.F., Storey, J.M., Storey, K.B., and Hermes-lima, M. (2011) Oxidative Stress in Estuarine and Intertidal Environments (Temperate and Tropical). In *Oxidative Stress in Aquatic Ecosystems*. Abele, D., Pablo, J., Vázquez-Medina, and Zenteno-Savín, T. (eds). Blackwell Publishing Ltd, pp. 41–57.

Fu, Y., Wang, Y., Gao, H., Li, D., Jiang, R., Ge, L., et al. (2021) Associations among Dietary

Omega-3 Polyunsaturated Fatty Acids, the Gut Microbiota, and Intestinal Immunity. *Mediators Inflamm* **2021**:.

Galano, J.M., Lee, Y.Y., Oger, C., Vigor, C., Vercauteren, J., Durand, T., et al. (2017) Isoprostanes, neuroprostanes and phytoprostanes: An overview of 25 years of research in chemistry and biology. *Prog Lipid Res* **68**: 83–108.

Garren, M., Son, K., Tout, J., Seymour, J.R., and Stocker, R. (2016) Temperature-induced behavioral switches in a bacterial coral pathogen. *ISME J* **10**: 1363–1372.

Garrity, S.D. (1984) Some adaptations of gastropods to physical stress on a tropical rocky shore. *Ecology* **65**: 559–574.

Giomi, F., Mandaglio, C., Ganmanee, M., Han, G.D., Dong, Y., Williams, G.A., and Sara, G. (2016) The importance of thermal history: Costs and benefits of heat exposure in a tropical, rocky shore oyster. *J Exp Biol* **219**: 686–694.

Green, T.J. and Barnes, A.C. (2010) Bacterial diversity of the digestive gland of Sydney rock oysters, *Saccostrea glomerata* infected with the paramyxean parasite, *Marteilia sydneyi*. *J Appl Microbiol* **109**: 613–622.

Harley, C.D.G. (2008) Tidal dynamics, topographic orientation, and temperature-mediated mass mortalities on rocky shores. *Mar Ecol Prog Ser* **371**: 37–46.

Hartman, L.M., van Oppen, M.J.H., and Blackall, L.L. (2020) The effect of thermal stress on the bacterial microbiome of *Exaiptasia diaphana*. *Microorganisms* **8**: 1–18.

Helmuth, B. and Hofmann, G.E. (2001) Microhabitats, thermal heterogeneity, and patterns of physiological stress in the rocky intertidal zone. *Biol Bull* **201**: 374–384.

Herlemann, D.P.R., Labrenz, M., Jürgens, K., Bertilsson, S., Waniek, J.J., and Andersson, A.F. (2011) Transitions in bacterial communities along the 2000 km salinity gradient of the Baltic Sea. *ISME J* **5**: 1571–1579.

Hermes-Lima, M., Moreira, D.C., Rivera-Ingraham, G.A., Giraud-Billoud, M., Genaro-Mattos, T.C., and Campos, É.G. (2015) Preparation for oxidative stress under hypoxia and metabolic depression: Revisiting the proposal two decades later. *Free Radic Biol Med* **89**: 1122–1143.

Hermes-Lima, M. and Zenteno-Savín, T. (2002) Animal response to drastic changes in oxygen availability and physiological oxidative stress. *Comp Biochem Physiol - C Toxicol Pharmacol* **133**: 537–556.

Herrera, M., Klein, S.G., Schmidt-Roach, S., Campana, S., Cziesielski, M.J., Chen, J.E., et al. (2020) Unfamiliar partnerships limit cnidarian holobiont acclimation to warming. *Glob Chang Biol* **26**: 5539–5553.

Hui, T.Y., Dong, Y., Han, G.D., Lau, S.L.Y., Cheng, M.C.F., Meepoka, C., et al. (2020) Timing metabolic depression: Predicting thermal stress in extreme intertidal environments. *Am Nat* **196**: 501–511.

Huyben, D., Roehe, B.K., Bekaert, M., Ruyter, B., and Glencross, B. (2020) Dietary lipid:Protein ratio and n-3 long-chain polyunsaturated fatty acids alters the gut microbiome of Atlantic salmon under hypoxic and normoxic conditions. *Front Microbiol* **11**: 589898.

Jaramillo, A. and Castañeda, L.E. (2021) Gut Microbiota of Drosophila subobscura Contributes to Its Heat Tolerance and Is Sensitive to Transient Thermal Stress. *Front Microbiol* **12**: 1–13.

Jiang, Y., Jiao, H., Sun, P., Yin, F., and Tang, B. (2020) Metabolic response of Scapharca subcrenata to heat stress using GC/MS-based metabolomics. *PeerJ* **2020**: 1–20.

Kandlikar, G.S., Gold, Z.J., Cowen, M.C., Meyer, R.S., Freise, A.C., Kraft, N.J.B., et al. (2018) Ranacapa: An R package and shiny web app to explore environmental DNA data with exploratory statistics and interactive visualizations. *F1000Research* **7**: 1–19.

Kers, J.G. and Saccenti, E. (2022) The Power of Microbiome Studies: Some Considerations

on Which Alpha and Beta Metrics to Use and How to Report Results. *Front Microbiol* **12**: 1–18.
King, G.M., Judd, C., Kuske, C.R., and Smith, C. (2012) Analysis of stomach and gut microbiomes of the Eastern oyster (*Crassostrea virginica*) from Coastal Louisiana, USA. *PLoS One* **7**:.
Klindworth, A., Pruesse, E., Schweer, T., Peplies, J., Quast, C., Horn, M., and Glöckner, F.O. (2013) Evaluation of general 16S ribosomal RNA gene PCR primers for classical and next-generation sequencing-based diversity studies. *Nucleic Acids Res* **41**: 1–11.
Kodama, Y. and Watanabe, K. (2004) *Sulfuricurvum kujiense* gen. nov., sp. nov., a facultatively anaerobic, chemolithoautotrophic, sulfur-oxidizing bacterium isolated from an underground crude-oil storage cavity. *Int J Syst Evol Microbiol* **54**: 2297–2300.
Kremer, N., Koch, E.J., El Filali, A., Zhou, L., Heath-Heckman, E.A.C., Ruby, E.G., and McFall-Ngai, M.J. (2018) Persistent interactions with bacterial symbionts direct mature-host cell morphology and gene expression in the squid-*Vibrio* symbiosis. *mSystems* **3**: 1–17.
Lathlean, J.A., Ayre, D.J., and Minchinton, T.E. (2014) Estimating latitudinal variability in extreme heat stress on rocky intertidal shores. *J Biogeogr* **41**: 1478–1491.
Lau, N.S., Ting, S.Y., Sam, K.K., Janaranjani, M., Wong, S.C., Wu, X., et al. (2022) Comparative analyses of *Scylla olivacea* gut microbiota composition and function suggest the capacity for polyunsaturated fatty acid biosynthesis. *Microb Ecol* 1–14.
Lee, Y.Y., Galano, J.M., Leung, H.H., Balas, L., Oger, C., Durand, T., and Lee, J.C.Y. (2020) Nonenzymatic oxygenated metabolite of docosahexaenoic acid, 4(RS)-4-F_{4t}-neuroprostane, acts as a bioactive lipid molecule in neuronal cells. *FEBS Lett* **594**: 1797–1808.
Lee, Y.Y. and Lee, J.C.-Y. (2018) LC-MS/MS Analysis of Lipid Oxidation Products in Blood and Tissue Samples. In *Clinical Metabolomics: Methods and Protocols*. Giera, M. (ed). Springer Science+Business Media, LLC.
Lent, C.M. (1969) Adaptations of the ribbed mussel, Modiolus demissus (Dillvvyn), to the intertidal habitat. *Integr Comp Biol* **9**: 283–292.
Lenth, R. V. (2023) emmeans: Estimated Marginal Means, aka Least-Squares Means.
Leung, K.S., Galano, J.M., Durand, T., and Lee, J.C.Y. (2015) Current development in non-enzymatic lipid peroxidation products, isoprostanoids and isofuranoids, in novel biological samples. *Free Radic Res* **49**: 816–826.
Li, J., Bates, K.A., Hoang, K.L., Hector, T.E., Knowles, S.C.L., and King, K.C. (2022) Experimental temperatures shape host microbiome diversity and composition. *Glob Chang Biol* **00**: 1–16.
Li, Y.F., Yang, N., Liang, X., Yoshida, A., Osatomi, K., Power, D., et al. (2018) Elevated seawater temperatures decrease microbial diversity in the gut of *Mytilus coruscus*. *Front Physiol* **9**: 839.
Lin, H. and Peddada, S. Das (2020) Analysis of compositions of microbiomes with bias correction. *Nat Commun* **11**: 1–11.
Liu, M., Li, Q., Tan, L., Wang, L., Wu, F., Li, L., and Zhang, G. (2023) Host-microbiota interactions play a crucial role in oyster adaptation to rising seawater temperature in summer. *Environ Res* **216**:.
Lokmer, A. and Wegner, K.M. (2015) Hemolymph microbiome of Pacific oysters in response to temperature, temperature stress and infection. *ISME J* **9**: 670–682.
de Lorgeril, J., Lucasson, A., Petton, B., Toulza, E., Montagnani, C., Clerissi, C., et al. (2018) Immune-suppression by OsHV-1 viral infection causes fatal bacteraemia in Pacific oysters. *Nat Commun* **9**:.
Ma, K., Chen, S., Wu, Y., Ma, Y., Qiao, H., Fan, J., and Wu, H. (2022) Dietary

990 supplementation with microalgae enhances the zebrafish growth performance by
991 modulating immune status and gut microbiota. *Appl Microbiol Biotechnol* **106**: 773–788.
992 Maher, R.L., Schmeltzer, E.R., Meiling, S., McMinds, R., Ezzat, L., Shantz, A.A., et al.
993 (2020) Coral microbiomes demonstrate flexibility and resilience through a reduction in
994 community diversity following a thermal stress event. *Front Ecol Evol* **8**: 555698.
995 Mallick, H., Franzosa, E.A., Mclver, L.J., Banerjee, S., Sirota-Madi, A., Kostic, A.D., et al.
996 (2019) Predictive metabolomic profiling of microbial communities using amplicon or
997 metagenomic sequences. *Nat Commun* **10**: 1–11.
998 Mallott, E.K., Skovmand, L.H., Garber, P.A., and Amato, K.R. (2022) The fecal metabolome
999 of black howler monkeys (*Alouatta pigra*) varies in response to seasonal dietary changes.
1000 Marangon, E., Laffy, P.W., Bourne, D.G., and Webster, N.S. (2021) Microbiome-mediated
1001 mechanisms contributing to the environmental tolerance of reef invertebrate species.
1002 *Mar Biol* **168**: 1–18.
1003 Marshall, D.J., Dong, Y., McQuaid, C.D., and Williams, G.A. (2011) Thermal adaptation in
1004 the intertidal snail *Echinolittorina malaccana* contradicts current theory by revealing the
1005 crucial roles of resting metabolism. *J Exp Biol* **214**: 3649–3657.
1006 Marshall, D.J. and McQuaid, C.D. (2011) Warming reduces metabolic rate in marine snails:
1007 Adaptation to fluctuating high temperatures challenges the metabolic theory of ecology.
1008 *Proc R Soc B Biol Sci* **278**: 281–288.
1009 Masasa, M., Kushmaro, A., Nguyen, D., Chernova, H., Shashar, N., and Guttman, L. (2023)
1010 Spatial Succession Underlies Microbial Contribution to Food Digestion in the Gut of an
1011 Algivorous Sea. *Am Soc Microbiol*.
1012 Maurice, C.F., Cl Knowles, S., Ladau, J., Pollard, K.S., Fenton, A., Pedersen, A.B., and
1013 Turnbaugh, P.J. (2015) Marked seasonal variation in the wild mouse gut microbiota.
1014 *ISME J* **9**: 2423–2434.
1015 McDevitt-Irwin, J.M., Garren, M., McMinds, R., Vega Thurber, R., and Baum, J.K. (2019)
1016 Variable interaction outcomes of local disturbance and El Niño-induced heat stress on
1017 coral microbiome alpha and beta diversity. *Coral Reefs* **38**: 331–345.
1018 McKnight, D.T., Huerlimann, R., Bower, D.S., Schwarzkopf, L., Alford, R.A., and Zenger,
1019 K.R. (2019) Methods for normalizing microbiome data: An ecological perspective.
1020 *Methods Ecol Evol* **10**: 389–400.
1021 Mcmahon, B.R. (1988) Physiological responses to oxygen depletion in intertidal animals.
1022 *Integr Comp Biol* **28**: 39–53.
1023 McMurdie, P.J. and Holmes, S. (2013) Phyloseq: An R Package for reproducible interactive
1024 analysis and graphics of microbiome census data. *PLoS One* **8**:.
1025 Mekuchi, M., Asakura, T., Sakata, K., Yamaguchi, T., Teruya, K., and Kikuchi, J. (2018)
1026 Intestinal microbiota composition is altered according to nutritional biorhythms in the
1027 leopard coral grouper (Plectropomus leopardus). *PLoS One* **13**: 1–16.
1028 Miller, E., Morel, A., Saso, L., and Saluk, J. (2014) Isoprostanes and neuroprostanes as
1029 biomarkers of oxidative stress in neurodegenerative diseases. *Oxid Med Cell Longev*
1030 **2014**:.
1031 Monroig, Shu-Chien, A.C., Kabeya, N., Tocher, D.R., and Castro, L.F.C. (2022) Desaturases
1032 and elongases involved in long-chain polyunsaturated fatty acid biosynthesis in aquatic
1033 animals: From genes to functions. *Prog Lipid Res* **86**: 101157.
1034 Le Moullac, G., Cheize, M., Gastineau, O., Daniel, J.Y., Le Coz, J.R., Huvet, A., et al. (2008)
1035 Ecophysiological and metabolic adaptations to sulphide exposure of the oyster
1036 *Crassostrea gigas*. *J Shellfish Res* **27**: 355–363.
1037 Muñoz, K., Flores-Herrera, P., Gonçalves, A.T., Rojas, C., Yáñez, C., Mercado, L., et al.
1038 (2019) The immune response of the scallop *Argopecten purpuratus* is associated with
1039 changes in the host microbiota structure and diversity. *Fish Shellfish Immunol* **91**: 241–

250.
Nakagawa, S., Saito, H., Tame, A., Hirai, M., Yamaguchi, H., Sunata, T., et al. (2017) Microbiota in the coelomic fluid of two common coastal starfish species and characterization of an abundant *Helicobacter*-related taxon. *Sci Rep* **7**: 1–10.
Nearing, J.T., Douglas, G.M., Hayes, M., Macdonald, J., Desai, D., Allward, N., et al. (2022) Microbiome differential abundance methods produce disturbingly different results across 38 datasets. *Nat Commun* **13**: 342.
Neu, A.T., Hughes, I. V., Allen, E.E., and Roy, K. (2021) Decade-scale stability and change in a marine bivalve microbiome. *Mol Ecol* **30**: 1237–1250.
Ng, T.P.T., Lau, S.L.Y., Davies, M.S., Stafford, R., Seuront, L., Hutchinson, N., et al. (2021) Behavioral repertoire of high-shore littorinid snails reveals novel adaptations to an extreme environment. *Ecol Evol* **11**: 7114–7124.
Ng, T.P.T., Lau, S.L.Y., Seuront, L., Davies, M.S., Stafford, R., Marshall, D.J., and Williams, G.A. (2017) Linking behaviour and climate change in intertidal ectotherms: insights from littorinid snails. *J Exp Mar Bio Ecol* **492**: 121–131.
Nguyen, Q.P., Karagas, M.R., Madan, J.C., Dade, E., Palys, T.J., Morrison, H.G., et al. (2021) Associations between the gut microbiome and metabolome in early life. *BMC Microbiol* **21**: 1–19.
Nicastro, K.R., Zardi, G.I., McQuaid, C.D., Stephens, L., Radloff, S., and Blatch, G.L. (2010) The role of gaping behaviour in habitat partitioning between coexisting intertidal mussels. *BMC Ecol* **10**:.
Oksanen, J., Simpson, G.L., Blanchet, F.G., Kindt, R., Legendre, P., Minchin, P.R., et al. (2022) Vegan: community ecology package. *R Packag version 26-2*.
Pal, V.K., Bandyopadhyay, P., and Singh, A. (2018) Hydrogen sulfide in physiology and pathogenesis of bacteria and viruses. *IUBMB Life* **70**: 393–410.
Parris, D.J., Morgan, M.M., and Stewart, F.J. (2019) Feeding rapidly alters microbiome composition and gene transcription in the clownfish gut. *Appl Environ Microbiol* **85**: 1–15.
Petersen, C. and Round, J.L. (2014) Defining dysbiosis and its influence on host immunity and disease. *Cell Microbiol* **16**: 1024–1033.
Pierce, M.L. and Evan, J. (2019) Gut microbiomes of the eastern oyster (*Crassostrea virginica*) and the blue mussel (*Mytilus edulis*): Temporal variation and the influence of marine aggregate-associated microbial communities. *mSphere* **4**: e00730-19.
Pierce, M.L. and Ward, J.E. (2018) Microbial Ecology of the Bivalvia, with an Emphasis on the Family Ostreidae. *J Shellfish Res* **37**: 793–806.
Pimentel, Z.T., Dufault-Thompson, K., Russo, K.T., Scro, A.K., Smolowitz, R.M., Gomez-Chiarri, M., and Zhang, Y. (2021) Microbiome analysis reveals diversity and function of *Mollicutes* associated with the Eastern oyster, Crassostrea virginica. *mSphere* **6**: e00227-21.
Pita, L., Rix, L., Slaby, B.M., Franke, A., and Hentschel, U. (2018) The sponge holobiont in a changing ocean: from microbes to ecosystems. *Microbiome* **6**: 46.
Qi, Z. and Voit, E.O. (2017) Strategies for Comparing Metabolic Profiles: Implications for the Inference of Biochemical Mechanisms from Metabolomics Data. *IEEE/ACM Trans Comput Biol Bioinform* **14**: 1434–1445.
Quast, C., Pruesse, E., Yilmaz, P., Gerken, J., Schweer, T., Yarza, P., et al. (2013) The SILVA ribosomal RNA gene database project: Improved data processing and web-based tools. *Nucleic Acids Res* **41**: D590–D596.
Rädecker, N., Pogoreutz, C., Gegner, H.M., Cárdenas, A., Perna, G., Geißler, L., et al. (2022) Heat stress reduces the contribution of diazotrophs to coral holobiont nitrogen cycling. *ISME J* **16**: 1110–1118.

1090 Raffaelli, D. and Hawkins, S. (1999) Intertidal ecology, 2nd ed. Kluwer Academic Publishers.
1091 Rocca, J.D., Simonin, M., Blaszczak, J.R., Ernakovich, J.G., Gibbons, S.M., Midani, F.S., and
1092 Washburne, A.D. (2019) The Microbiome Stress Project: Toward a global meta-analysis
1093 of environmental stressors and their effects on microbial communities. *Front Microbiol*
1094 **9**: 3272.
1095 Roy, J., Galano, J.M., Durand, T., Le Guennec, J.Y., and Lee, J.C.Y. (2017) Physiological
1096 role of reactive oxygen species as promoters of natural defenses. *FASEB J* **31**: 3729–
1097 3745.
1098 Samakraman, S., Williams, G.A., and Ganmanee, M. (2010) Spatial and temporal variability
1099 of intertidal rocky shore molluscs in Sichang Island, East Coast of Thailand. *Publ Seto*
1100 *Mar Biol Lab* **10**: 35–46.
1101 Santoro, E.P., Borges, R.M., Espinoza, J.L., Freire, M., Messias, C.S.M.A., Villela, H.D.M.,
1102 et al. (2021) Coral microbiome manipulation elicits metabolic and genetic restructuring
1103 to mitigate heat stress and evade mortality. *Sci Adv* **7**: 19–21.
1104 Sargent, J.R. (1976) The Structure, Metabolism and Function of Lipids in Marine organisms.
1105 In *Biochemical and biophysical perspectives in marine biology*. Malins, D.C. and
1106 Sargent, J.R. (eds). New York: Academic Press, pp. 149–212.
1107 Scanes, E., Parker, L.M., Seymour, J.R., Siboni, N., Dove, M.C., O'Connor, W.A., and Ross,
1108 P.M. (2021) Microbiomes of an oyster are shaped by metabolism and environment. *Sci*
1109 *Rep* **11**: 1–7.
1110 Segata, N., Izard, J., Waldron, L., Gevers, D., Miropolsky, L., Garrett, W.S., and
1111 Huttenhower, C. (2011) Metagenomic biomarker discovery and explanation. *Genome*
1112 *Biol* **12**: R60.
1113 Sepulveda, J. and Moeller, A.H. (2020) The effects of temperature on animal gut
1114 microbiomes. *Front Microbiol* **11**: 384.
1115 Sharp, C. and Foster, K.R. (2022) Host control and the evolution of cooperation in host
1116 microbiomes. *Nat Commun* **13**: 1–15.
1117 Sharp, K.H., Pratte, Z.A., Kerwin, A.H., Rotjan, R.D., and Stewart, F.J. (2017) Season, but
1118 not symbiont state, drives microbiome structure in the temperate coral *Astrangia*
1119 *poculata*. *Microbiome* **5**: 120.
1120 Shaver, E.C., Shantz, A.A., McMinds, R., Burkepile, D.E., Thurber, R.L.V., and Silliman,
1121 B.R. (2017) Effects of predation and nutrient enrichment on the success and microbiome
1122 of a foundational coral. *Ecology* **98**: 830–839.
1123 Shiu, J.H., Keshavmurthy, S., Chiang, P.W., Chen, H.J., Lou, S.P., Tseng, C.H., et al. (2017)
1124 Dynamics of coral-associated bacterial communities acclimated to temperature stress
1125 based on recent thermal history. *Sci Rep* **7**: 1–13.
1126 Soen, Y. (2014) Environmental disruption of host-microbe co-adaptation as a potential
1127 driving force in evolution. *Front Genet* **5**: 168.
1128 Sokolova, I.M. and Pörtner, H.O. (2001) Physiological adaptations to high intertidal life
1129 involve improved water conservation abilities and metabolic rate depression in *Littorina*
1130 *saxatilis*. *Mar Ecol Prog Ser* **224**: 171–186.
1131 Sokolova, I.M., Sukhotin, A.A., and Lannig, G. (2011) Marine Animal Stress Response and
1132 Biomonitoring and Energy Budgets In Mollusks. In *Oxidative stress in aquatic*
1133 *ecosystems*. pp. 261–280.
1134 Somero, G.N. (2002) Thermal physiology and vertical zonation of intertidal animals: Optima,
1135 limits, and costs of living. *Integr Comp Biol* **42**: 780–789.
1136 Sorek, M., Díaz-Almeyda, E.M., Medina, M., and Levy, O. (2014) Circadian clocks in
1137 symbiotic corals: The duet between *Symbiodinium* algae and their coral host. *Mar*
1138 *Genomics* **14**: 47–57.
1139 Stevick, R.J., Post, A.F., and Gómez-Chiarri, M. (2021) Functional plasticity in oyster gut

1140 microbiomes along a eutrophication gradient in an urbanized estuary. *Anim Microbiome*
1141 **3**:.
1142 Stillman, J.H. (2002) Causes and consequences of thermal tolerance limits in rocky intertidal
1143 porcelain crabs, genus *Petrolisthes*. *Integr Comp Biol* **42**: 790–796.
1144 Storey, K.B. and Storey, J.M. (2004) Oxygen Limitation and Metabolic Rate Depression. In
1145 *Functional Metabolism: Regulation and Adaptation*. John Wiley & Sons, Inc.
1146 Tremaroli, V. and Bäckhed, F. (2012) Functional interactions between the gut microbiota and
1147 host metabolism. *Nature* **489**: 242–249.
1148 Vandamme, P. and De Ley, J. (1991) Proposal for a new family, *Campylobacteraceae*. *Int J*
1149 *Syst Bacteriol* **41**: 451–455.
1150 Voolstra, C.R. and Ziegler, M. (2020) Adapting with microbial help: Microbiome flexibility
1151 facilitates rapid responses to environmental change. *BioEssays* **42**: 1–9.
1152 Walke, J.B., Becker, M.H., Krinos, A., Chang, E.A.B., Santiago, C., Umile, T.P., et al. (2021)
1153 Seasonal changes and the unexpected impact of environmental disturbance on skin
1154 bacteria of individual amphibians in a natural habitat. *FEMS Microbiol Ecol* **97**: 1–14.
1155 Wang, J., Ma, L.X., and Dong, Y.W. (2022) Coping with harsh heat environments: molecular
1156 adaptation of metabolic depression in the intertidal snail *Echinolittorina radiata*. *Cell*
1157 *Stress Chaperones*.
1158 Weiss, S., Xu, Z.Z., Peddada, S., Amir, A., Bittinger, K., Gonzalez, A., et al. (2017)
1159 Normalization and microbial differential abundance strategies depend upon data
1160 characteristics. *Microbiome* **5**: 1–18.
1161 Welker, A.F., Moreira, D.C., Campos, É.G., and Hermes-Lima, M. (2013) Role of redox
1162 metabolism for adaptation of aquatic animals to drastic changes in oxygen availability.
1163 *Comp Biochem Physiol - A Mol Integr Physiol* **165**: 384–404.
1164 Wickham, H. (2008) ggplot2: Elegant Graphics for Data Analysis, New York, USA: Springer
1165 Science+Business Media, LCC.
1166 Williams, E.E. and Somero, G.N. (1996) Seasonal-, tidal-cycle- and microhabitat-related
1167 variation in membrane order of phospholipid vesicles from gills of the intertidal mussel
1168 Mytilus californianus. *J Exp Biol* **199**: 1587–1596.
1169 Williams, G.A. and Morritt, D. (1995) Habitat partitioning and thermal tolerance in a tropical
1170 limpet, Cellana grata. *Mar Ecol Prog Ser* **124**: 89–103.
1171 Willis, A.D. (2019) Rarefaction, alpha diversity, and statistics. *Front Microbiol* **10**:.
1172 Yin, X., Chen, P., Chen, H., Jin, W., and Yan, X. (2017) Physiological performance of the
1173 intertidal Manila clam (*Ruditapes philippinarum*) to long-term daily rhythms of air
1174 exposure. *Sci Rep* **7**: 41648.
1175 Yonny, M.E., Rodríguez Torresi, A., Cuyamendous, C., Réversat, G., Oger, C., Galano, J.M.,
1176 et al. (2016) Thermal stress in melon plants: Phytoprostanes and phytofurans as
1177 oxidative stress biomarkers and the effect of antioxidant supplementation. *J Agric Food*
1178 *Chem* **64**: 8296–8304.
1179 Zaneveld, J.R., McMinds, R., and Thurber, R.V. (2017) Stress and stability: Applying the
1180 Anna Karenina principle to animal microbiomes. *Nat Microbiol* **2**:.
1181 Ziegler, M., Seneca, F.O., Yum, L.K., Palumbi, S.R., and Voolstra, C.R. (2017) Bacterial
1182 community dynamics are linked to patterns of coral heat tolerance. *Nat Commun* **8**: 1–8.
1183
1184

Supplementary information

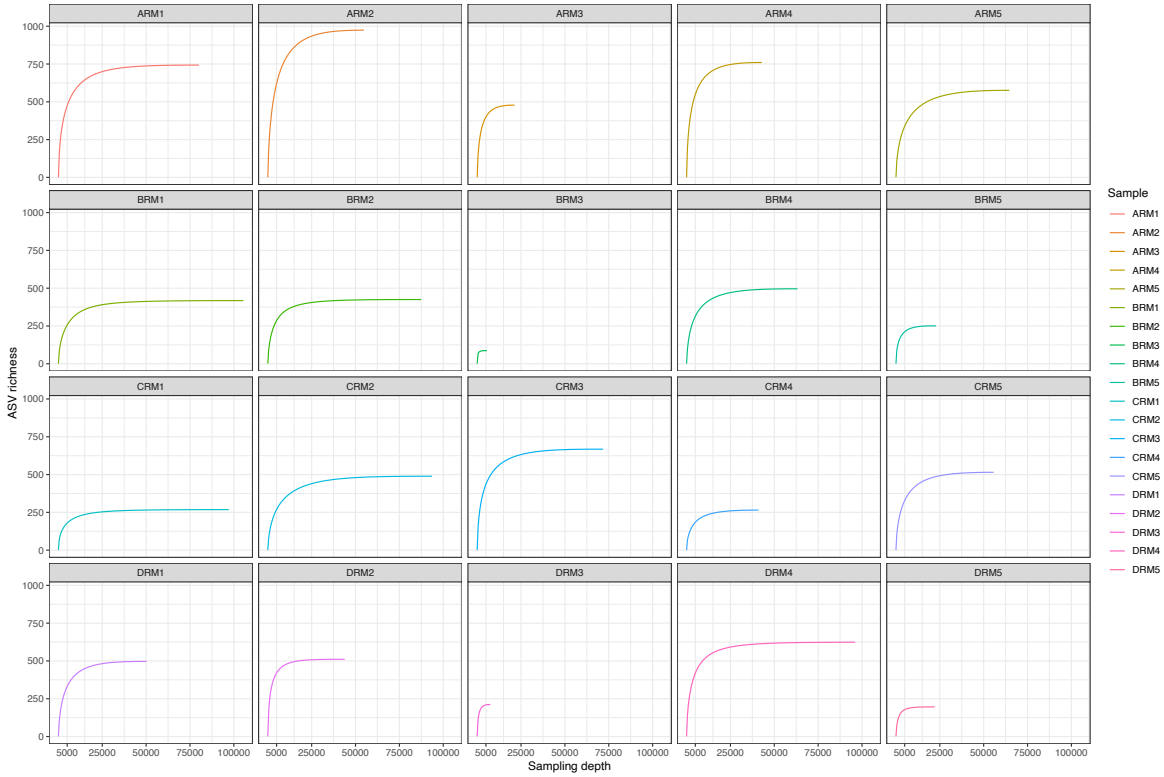

Fig. S1. Rarefaction curves illustrating the ASVs captured against the sampling depth which was generated for each sample using their corresponding quality-filtered V3-V4 16SrRNA sequences.

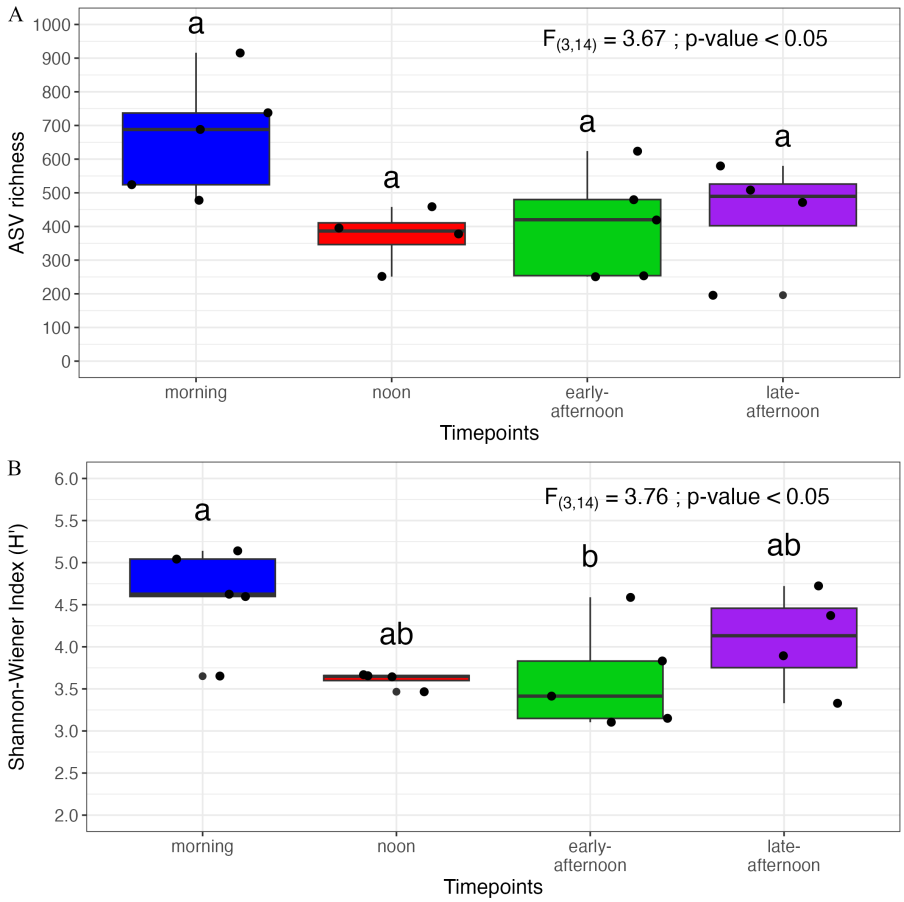

Fig. S2. *I. nucleus*-associated microbiome ASV richness and Shannon-Wiener diversity across the emersion period. Boxplot showing the alpha diversity index of (A) ASV richness, and (B) Shannon-Wiener index (H') of the oyster-associated microbiome at different timepoints. (Centre line represents the median; box limits indicate the first and third quartiles; the lower and upper whiskers indicate the smallest and largest values that within 1.5 times of the IQR (Inter-quartile range) from the first and third quartiles, respectively. The data points shown in each timepoint is replicate values. Statistical significance ($p < 0.05$) is indicated if the letters above each boxplot are different between any two timepoints.

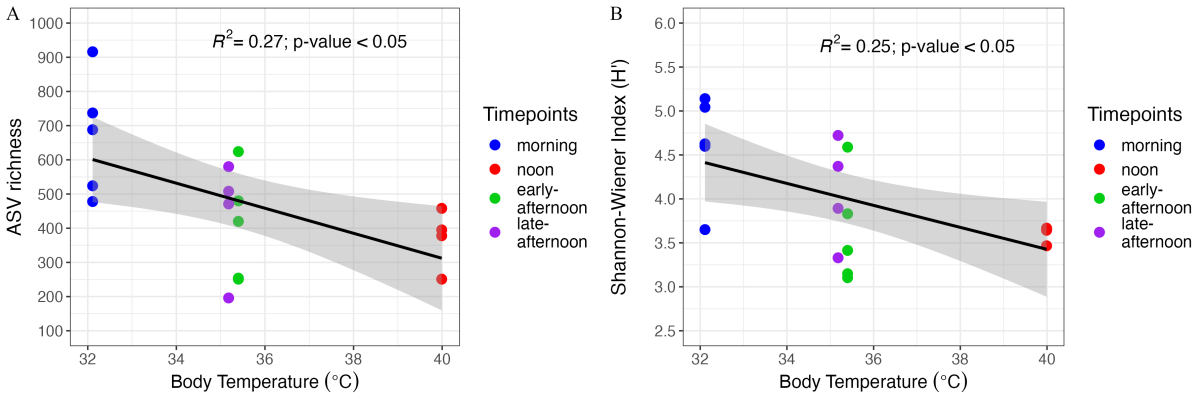

Fig. S3. Variation in the alpha diversity indices of the *I. nucleus*-associated microbiome can be explained by the host body temperature. Linear regression graph showing the relationship between average body temperature (from 10 random independent replicates collected at each timepoint) and (A) ASV richness (B) Shannon-Wiener index (H'). The

datapoints shown in each panel were the samples' replicates (n= 4-5) from their corresponding timepoint. The shaded grey area indicates a 95% confidence interval for the predicted regression line. Statistical result (least square regression analysis) is shown in the upper right within each panel.

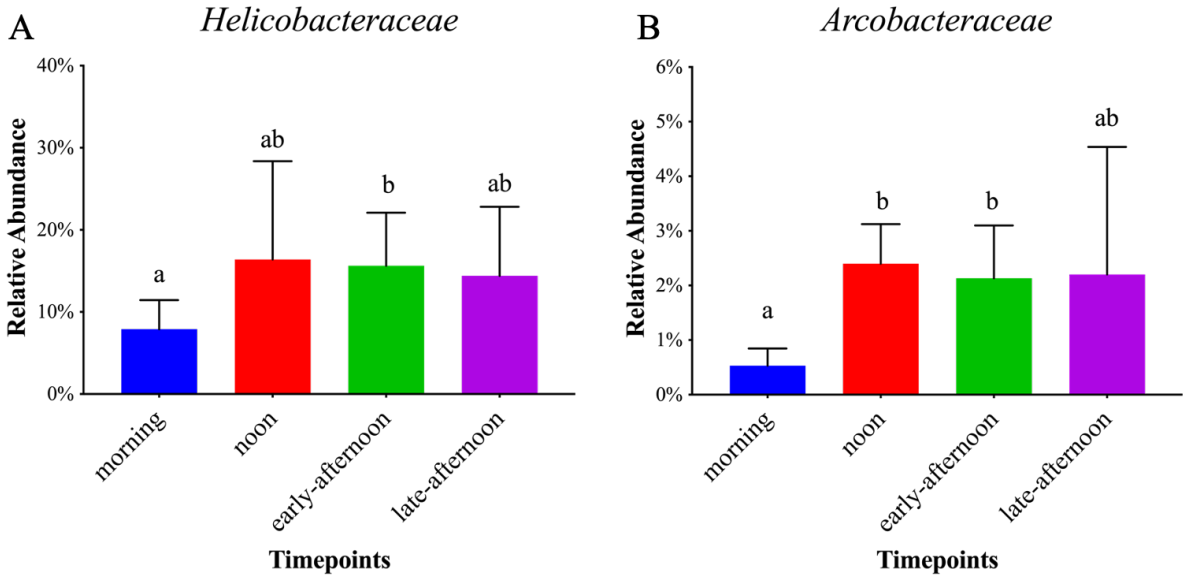

Fig. S4. *Helicobacteraceae* and *Arcobacteraceae* mean relative abundance vary across the emersion period. Bar graphs showing the two dominant family level taxa in *I. nucleus*'s gut microbiome at each timepoint: (A) *Helicobacteraceae* (B) *Arcobacteraceae*. Data are presented as mean relative abundance and + 1 standard deviation (error bar) for each taxon at the given timepoints. Statistical significance (p-value < 0.05) is indicated if the letters above each bar are different

.

1223 Table S1. Metadata describing the *Isognomon nucleus* samples' collected information

Date	Time	Timepoints label	Replicates	Sample name	Body (mm)
22.05.2019	0915	morning	1	ARM1	12.9
			2	ARM2	13.5
			3	ARM3	15.2
			4	ARM4	12.5
			5	ARM5	13.7
	1230	noon	1	BRM1	11.7
			2	BRM2	11.3
			4	BRM4	11.9
			5	BRM5	12.4
	1612	early-afternoon	1	CRM1	11.7
			2	CRM2	12.9
			3	CRM3	13.0
			4	CRM4	12.0
			5	CRM5	11.7
	1740	late-afternoon	1	DRM1	11.8
			2	DRM2	10.9
			4	DRM4	11.1
			5	DRM5	11.9

1224

1225 Table S2. Description of oxidized poly-unsaturated fatty acids (PUFA) products

PUFA	Oxidized PUFA products
Arachidonic acid (ARA)	5-F_{2t}-IsoP
	15-F_{2t}-IsoP
Adrenic acid (AdA)	7-F_{2t}-Dihomo-IsoP
	17-F_{2t}-Dihomo-IsoP
Docosahexaenoic acid (DHA)	4-F_{4t}-NeuroP
	10-F_{4t}-NeuroP
	13-F_{4t}-NeuroP
	20-F_{4t}-NeuroP
α-Linolenic acid (ALA)	9-D_{1t}-PhytoP
	9-F_{1t}-PhytoP
	16-F_{1t}-PhytoP
	16-B_{1t}-PhytoP
Eicosapentaenoic acid (EPA)	5-F_{3t}-IsoP
	15-F_{3t}-IsoP
	8-F_{3t}-IsoP

1226